Geophys. J. R. astr. Soc. (1987) **91**, 755–794

Multiple-taper spectral analysis of terrestrial free oscillations: part I

Jeffrey Park *Department of Geology and Geophysics Yale University, New Haven, CT 06511, USA*

Craig R. Lindberg *Institute of Geophysics and Planetary Physics, Scripps Institution of Oceanography, University of California, San Diego, CA 92093, USA*

David J. Thomson *Bell Laboratories, Murray Hill, NJ 07974, USA*

Accepted 1987 April 28. Received 1987 April 22; in original form 1986 September 3

Summary. We present a new method for estimating the frequencies of the Earth's free oscillations. This method is an extension of the techniques of Thomson (1982) for finding the harmonic components of a time series. Optimal tapers for reducing the spectral leakage of decaying sinusoids immersed in white noise are derived. Multiplying the data by the best K tapers creates K time series. A decaying sinusoid model is fit to the K time series by a least squares procedure. A statistical F-test is performed to test the fit of the decaying sinusoid model, and thus determine the probability that there are coherent oscillations in the data. The F-test is performed at a number of chosen frequencies, producing a measure of the certainty that there is a decaying sinusoid at each frequency. We compare this method with the conventional technique employing a discrete Fourier transform of a cosine-tapered time-series. The multiple-taper method is found to be a more sensitive detector of decaying sinusoids in a time series contaminated by white noise.

Key words: multiple-taper, free oscillations, spectral analysis

1 Introduction

The free oscillations of the Earth appear as decaying sinusoids in the records of instruments in the available low-frequency seismic arrays (International Deployment of Accelerometers, hereafter referred to as IDA, and Global Digital Seismic Network, hereafter referred to as GDSN) (Agnew *et al.* 1976; Engdahl, Peterson & Orsini 1982). Information about the structure of the Earth can be inferred from the frequencies, decay rates and amplitudes of these oscillations.

Conventionally, these characteristics of the decaying sinusoids are estimated from a direct spectral estimate of the data using a cosine taper (Harris 1978; Dahlen 1982; Lindberg 1986), or by producing spherical harmonic-weighted sums of the direct spectral estimates made

Downloaded from https://academic.oup.com/gji/article/91/3/755/641480 by guest on 21 August 2022

from each station's record ('stacking' or 'stripping') (Gilbert & Dziewonski 1975). There are several difficulties with using a single cosine-taper in the harmonic analysis of free oscillations. The time series analysed in free oscillation studies are non-stationary; they are also contaminated with noise. The cosine taper is symmetric and appropriate for stationary time-series; it is not a good taper for minimizing the spectral leakage of decaying sinusoids immersed in noise. The cosine taper also discards much of the data at the ends of the time series, particularly at the beginning where the signal-to-noise ratios of the free oscillation records are large. This is not desirable. In addition, applying a cosine taper to reduce spectral leakage is purchased with greatly increased variance (e.g. figs 7 and 8 of Dahlen 1982). Use of the cosine taper roughly doubles the variance, or equivalently, halves statistical efficiency of the estimate (Jones 1962). Another drawback of a cosine-taper direct spectral estimate is that it does not discriminate between oscillations of constant phase and frequency (harmonic oscillations) and broad distributions of spectral energy caused by other processes.

To overcome these problems, we have developed a method of harmonic analysis for decaying sinusoids immersed in stationary white noise based on the methods developed by Thomson (1982). A set of several 'optimal' tapers is created, each one designed to minimize the spectral leakage of decaying sinusoids immersed in white noise, while maintaining a large value for the ratio of tapered signal energy to tapered noise energy. Multiplying the data by each taper in turn creates several time series. Taking the discrete Fourier transform of these time series yields several complex eigenspectra (called eigencoefficients by Thomson 1982). A decaying sinusoid model is fit by a least-squares procedure to these complex eigenspectra. The least-squares procedure produces an estimate of the initial amplitude of any decaying sinusoids in the data. The fit of the decaying sinusoid model at any given frequency is tested using a statistical F-test. This gives a quantitative measure of the confidence that a phase-coherent decaying sinusoid is present in the data at any given frequency.

The multiple-taper method utilizes more of the data than the cosine-taper direct spectral estimate, and, as shown in Section 4 and the appendix, is a more sensitive detector of free oscillations in a seismic record. In one example, the five singlets of ${}_0S_2$ could be detected in a single record of the 1977 Sumbawa event, with measured frequencies in good agreement with those reported by Buland, Berger & Gilbert (1979), who used a six-station global array stack. Only two of the singlet lines are visible in the conventional direct spectral estimate employing a cosine taper.

The multiple-taper technique for free-oscillation analysis is described in the following sections. Section 2 introduces the functionals which are optimized to yield a family of spectral leakage-suppressing eigentapers appropriate for an oscillation with a given attenuation rate. Functionals for decaying sinusoids in time series with and without white noise are discussed. Section 3 introduces the statistical F-test for detection of decaying sinusoids. In Section 4 we present a number of frequency measurements of isolated free oscillations using IDA network data. Our conclusions are summarized in Section 5. An error analysis of the method is included in the appendix. Readers interested primarily in the examples are directed to Section 4. To implement the technique on a computer one needs to solve (2.19) to design the tapers, apply (3.15) to estimate the decaying sinusoid amplitudes as a function of frequency, and compute (3.28) to produce an F-test plot to test for the existence of decaying sinusoids at any given frequency.

2 Optimal data tapers for decaying signals

In this section we adapt the methods described in a series of five papers by Slepian, Landau and Pollak (Slepian & Pollak 1961; Landau & Pollak 1961, 1962; Slepian 1964, 1978). Their

Downloaded from https://academic.oup.com/gji/article/91/3/755/641480 by guest on 21 August 2022

work involved a set of time-limited functions whose spectral energy is optimally concentrated within a given frequency band. These functions have been employed to design optimal tapers for the analysis of stationary processes (Thomson 1982). We have extended Thomson's work to produce tapers for the harmonic analysis of exponentially decaying signals. For signals that decay exponentially with time, we obtain an optimization equation from which one can find the data taper w_0 with optimal resistance to spectral leakage from outside a frequency band of chosen width. Solving the optimization equation, one discovers that there exists a family of data tapers $\{w_0(t), w_1(t), \ldots, w_{k-1}(t)\}$ with good spectral-leakage resistance. We refer to the members of this family as eigentapers. These tapers are eigenvectors of a Toeplitz matrix whose elements are values taken by the function $\sin x/x$. In the next section we produce several spectra from a single record multiplied by each of the eigentapers in turn, and we show how these spectra can be combined to provide useful information.

An important factor in the analysis of low-frequency seismic data is the presence of stationary white noise in the records. This was recognized by Dahlen (1982); the presence of stationary noise determined the optimal time-series length for estimation of parameters in Dahlen's analysis. In his work, however, the taper shapes were held fixed. In this study, we extend the methods of Thomson (1982) to derive optimal taper shapes for any length time series, characterized by a parameter depending on the signal-to-noise ratio at the start of the seismic record. These 'noise-cognizant' tapers have less resistance to spectral leakage than those designed using a procedure that ignores stationary noise. In the appendix we show how noise-cognizant tapers improve the sensitivity of the eigentaper analysis if stationary noise is present in the data.

2A DECAYING SIGNAL WITH NO NOISE

Consider first a signal $x(t)$ that consists of a sum of decaying sinusoids uncorrupted by noise. Then one can represent

$$x(t) = \sum_j \mu_j \exp(i\omega_j t - \alpha_j t); \qquad t \geqslant 0,$$

where μ_j is the complex amplitude of the jth decaying sinusoid, which has angular frequency ω_j and decay rate α_j. In practice, one cannot measure $x(t)$, but only the N discrete numbers $x(t_0), x(t_1), \ldots, x(t_{N-1})$. Assume that $t_0 = 0$, and the time between samples $\Delta t = t_{j+1} - t_j$ is a constant, which we scale to be unity. If $\Delta t = 1$, then the Nyquist frequency $f_{\text{Nyquist}} = \frac{1}{2}$, and the angular frequency $\omega = 2\pi f$ is defined on its principal domain $(-\pi, \pi]$. Tapering the time series $\{x(t)\}_{t=0}^{N-1}$ consists of multiplying it by a real valued sequence $\{w(t)\}_{t=0}^{N-1}$ (the taper). Taking the discrete Fourier transform of the tapered signal $\{x(t)w(t)\}_{t=0}^{N-1}$ yields the function

$$y(\omega) = \sum_{t=0}^{N-1} \exp(-i\omega t) w(t) x(t). \tag{2.1}$$

This sum may be quickly computed using the Fast Fourier Transform (FFT) algorithm (Cooley & Tukey 1965; Brigham 1974). A traditional estimate of the energy content of $x(t)$ as a function of frequency is given by $|y(\omega)|^2$, where $\{w(t)\}_{t=0}^{N-1}$ is a conventional taper (Hann, Hamming, Blackman-Harris, Morse no. 2, etc.; Harris 1978 describes many of the popular tapers). The finite length of the time series makes a boxcar taper implicit if $w(t) \equiv 1$

Downloaded from https://academic.oup.com/gji/article/91/3/755/641480 by guest on 21 August 2022

in (2.1). One wishes to choose $\{w(t)\}_{t=0}^{N-1}$ to facilitate determination of the frequency content of $x(t)$.

The primary purpose of a data taper is to minimize spectral leakage. That is, the spectral component of a tapered signal at frequency $\hat{\omega}$ should have minimal energy contribution from outside the interval $(\hat{\omega}-\Omega, \hat{\omega}+\Omega)$, where $0<2\Omega<2\pi$ is a chosen bandwidth. One must also prevent the energy at $\hat{\omega}$ from the leaking out to affect parts of the spectrum at other frequencies. Suppose that $x(t)$ consists of only one decaying sinusoid in $(\hat{\omega}-\Omega, \hat{\omega}+\Omega)$, with frequency $\hat{\omega}$. The tapered signal $\{w(t)\mu\exp(i\hat{\omega}t-\alpha t)\}_{t=0}^{N-1}$ should have as much of its energy as possible in $(\hat{\omega}-\Omega, \hat{\omega}+\Omega)$ relative to its total energy, which covers the entire band $(-\pi, \pi)$. One chooses a taper $\{w(t)\}_{t=0}^{N-1}$ to maximize the functional

$$f=\frac{\int_{\hat{\omega}-\Omega}^{\hat{\omega}+\Omega}|y(\omega)|^2 d\omega}{\int_{-\pi}^{\pi}|y(\omega)|^2 d\omega}, \tag{2.2}$$

where $y(\omega)$ is the discrete Fourier transform of $\{x(t)w(t)\}_{t=0}^{N-1}$:

$$y(\omega)=\mu\sum_{t=0}^{N-1}\exp(-i\omega t)\exp(i\hat{\omega}t)w(t)\exp(-\alpha t)$$

(Slepian 1983 describes how maximizing a similar functional yields solutions to the concentration problem, which is important in electrical engineering.) Since our time signal is limited to $[0, N-1]$, there is no way to confine completely the energy of its frequency transform to $(\hat{\omega}-\Omega, \hat{\omega}+\Omega)$. Therefore, the value f will always be less than unity.

We expand the numerator of (2.2)

$$\begin{aligned}\int_{\hat{\omega}-\Omega}^{\hat{\omega}+\Omega}|y(\omega)|^2 d\omega &= |\mu|^2\int_{-\Omega}^{\Omega}d\omega\sum_{t=0}^{N-1}\exp(-i\omega t)w(t)\exp(-at)\\ &\quad\times\sum_{s=0}^{N-1}\exp(i\omega s)w(s)\exp(-\alpha s)\\ &= 2|\mu|^2\sum_{t=0}^{N-1}\sum_{s=0}^{N-1}w(t)\exp(-\alpha t)\frac{\sin\Omega(s-t)}{(s-t)}\exp(-\alpha s)w(s)\end{aligned} \tag{2.3}$$

and use Parseval's theorem to expand the denominator

$$\int_{-\pi}^{\pi}d\omega|y(\omega)|^2=2\pi|\mu|^2\sum_{t=0}^{N-1}w(t)\exp(-2\alpha t)\,w(t) \tag{2.4}$$

so that (2.2) becomes dependent entirely on $w(0), w(1), \ldots, w(N-1)$ and simple functions. Define the N-vector $\mathbf{w}=[w(0), w(1), \ldots, w(N-1)]$, the matrix $\mathbf{A}$ with elements

$$A_{lm}=\frac{\sin\Omega(l-m)}{\pi(l-m)}\exp(-\alpha(l+m)); \qquad l, m=0, 1, \ldots, N-1$$

and the diagonal matrix $\mathbf{B}$, where $B_{lm}=\delta_{lm}\exp(-2\alpha l)$; $l, m=0, 1, \ldots, N-1$. (The symbol δ_{ab} is the Kronecker delta function; $\delta_{ab}=1$ if $a=b$, and 0 otherwise.) Then equation (2.2) can be written as

$$f(\mathbf{w})=\frac{\mathbf{w}\cdot\mathbf{A}\cdot\mathbf{w}}{\mathbf{w}\cdot\mathbf{B}\cdot\mathbf{w}}. \tag{2.5}$$

Downloaded from https://academic.oup.com/gji/article/91/3/755/641480 by guest on 21 August 2022

To find the taper that optimizes the functional f, set the variation of f with respect to $\mathbf{w}$ equal to zero

$$\delta f(\mathbf{w};\mathbf{h}) = \frac{d}{d\epsilon} f(\mathbf{w}+\epsilon\mathbf{h})\bigg|_{\epsilon=0} = 0$$

for all N-vectors $\mathbf{h}$ (Goldstein 1980, chapter 2; Smith 1974). Some algebra leads to the eigenvalue problem

$$\mathbf{A}\cdot\mathbf{w} - \lambda\mathbf{B}\cdot\mathbf{w} = 0, \tag{2.6}$$

where $\mathbf{A}, \mathbf{B}$ are $N \times N$ real symmetric matrices and the eigenvalue

$\lambda = f(\mathbf{w})$.

The eigenvalue λ is always less than unity, as can be seen from (2.2). The fractional spectral leakage of the signal at $\hat{\omega}$ outside the frequency band $(\hat{\omega}-\Omega, \hat{\omega}+\Omega)$ is $1-\lambda$. The taper $\mathbf{w}_0 = [w_0(0), w_0(1), \ldots, w_0(N-1)]$ corresponding to the largest eigenvalue λ_0 is the optimal taper for minimizing spectral leakage. The taper $\mathbf{w}_0$ has roughly the same shape as other popular tapers such as the Hann and Blackman-Harris tapers. (The taper $\mathbf{w}_0$ corresponds to the solid curve labelled '0' in Figs 1 and 2.) The largest eigenvalue λ_0 is almost 1; one finds that $\lambda_0 \approx 1 - (2.9 \times 10^{-10})$ for $N\Omega = 8\pi$. Moreover, there are several eigenvalues in the descending family $\lambda_0 > \lambda_1 > \lambda_2 > \ldots > \lambda_{N-1}$ that are very close to λ_0 and hence close to unity. The associated eigenvectors $\mathbf{w}_0, \mathbf{w}_1, \mathbf{w}_2, \ldots, \mathbf{w}_{N-1}$ form a sequence of 'eigentapers', the first few of which possess good spectral leakage resistance.

Let the decay rate $\alpha = 0$ in (2.6), noting that $\mathbf{A}$ and $\mathbf{B}$ depend on α. Then (2.6) becomes equation (2.9) of Thomson (1982); its solutions are optimal tapers for concentrating the energy of nondecaying sinusoids. As discussed by Slepian (1978) and Thomson (1982), the

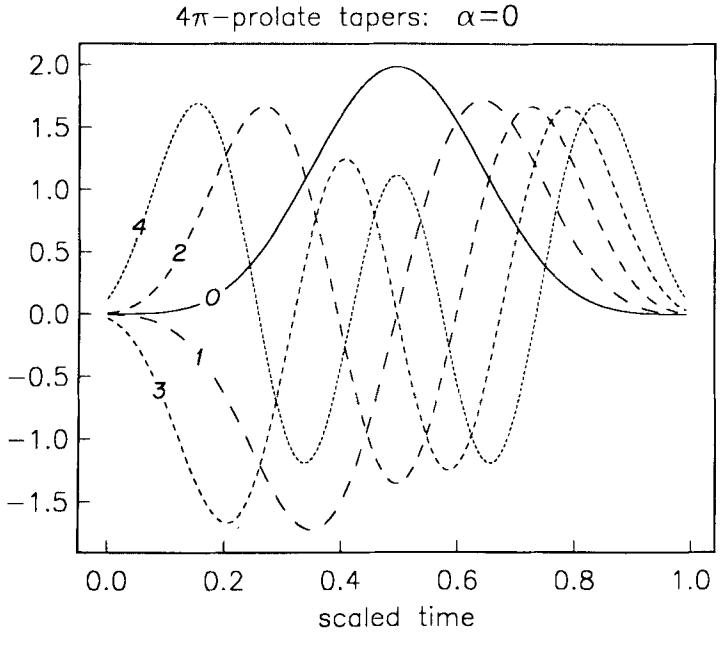

Figure 1. The five lowest-order eigentaper solutions to (2.6) when decay rate $\alpha = 0$, and $N\Omega = 8\pi$. The solid black line is the optimal taper. Higher order tapers are successively more oscillatory.

Downloaded from https://academic.oup.com/gji/article/91/3/755/641480 by guest on 21 August 2022

solutions to (2.6) when $\alpha = 0$ are the discrete $N \cdot W\pi$ prolate spheroidal sequences $\{v_t^{(k)}(N, W)\}_{t=0}^{N-1}$, where $W = \Omega/2\pi$ and k is an integer. If $\alpha \neq 0$, the solutions to (2.6) are the eigentapers $w_k(t) = v_t^{(k)}(N, \Omega/2\pi) \exp(\alpha t)$; $t = 0, 1, \ldots, N-1$. A spectral estimate using these tapers is similar to the 'analytic continuation' of the DFT discussed in Buland & Gilbert (1978). In much of the following, the time-bandwidth product $P = N \cdot W = N\Omega/2\pi = 4$. (In Slepian 1978, 1983, the parameter $c = \pi \cdot P$ is used.) P is usually taken to be an integer, but this convention is not required.

The $\{v_t^{(k)}(N, W)\}_{t=0}^{N-1}$ sequences have several properties that are shared with the decaying-signal eigentapers $\{w_k(t)\}_{t=0}^{N-1}$. For example, both possess an orthogonality property:

$$\sum_{t=0}^{N-1} v_t^{(k)}(N, W) v_t^{(k')}(N, W) = \sum_{t=0}^{N-1} \exp(-2\alpha t) w_k(t) w_{k'}(t) = \delta_{kk'}. \tag{2.7}$$

The tapers $\{w_k(t)\}_{t=0}^{N-1}$ sample that part of the signal that decays as $\exp(-\alpha t)$ in an orthogonal manner. Figure 1 shows the five lowest-order eigentapers $w_k(t) = v_t^{(k)}(N, W = 4/N)$; $t = 0, 1, \ldots, N-1$ for a stationary signal ($\alpha = 0$). The zeroth-order taper $\{w_0(t)\}_{t=0}^{N-1}$ is a 4π prolate taper. Note that the higher-order eigentapers are negative in some places and they weight the data more heavily near the ends of the record. Figure 2 shows eigentapers for a signal that decays by $\exp(-\pi\beta)$, where $\beta = \alpha T/\pi = 1.0$ Q-cycles, during the record length $T = N\Delta t$. [One Q-cycle refers to the time required for Q oscillations of the harmonic signal. This notation was introduced by Dahlen (1982). One Q-cycle is equivalent to an amplitude decay of $\exp(-\pi) \approx 1/23$]. Note the increasing amplitude towards the end of the record, as the tapers try to amplify the decaying signal. The tapers $\{w_k(t)\}_{t=0}^{N-1}$ produce the

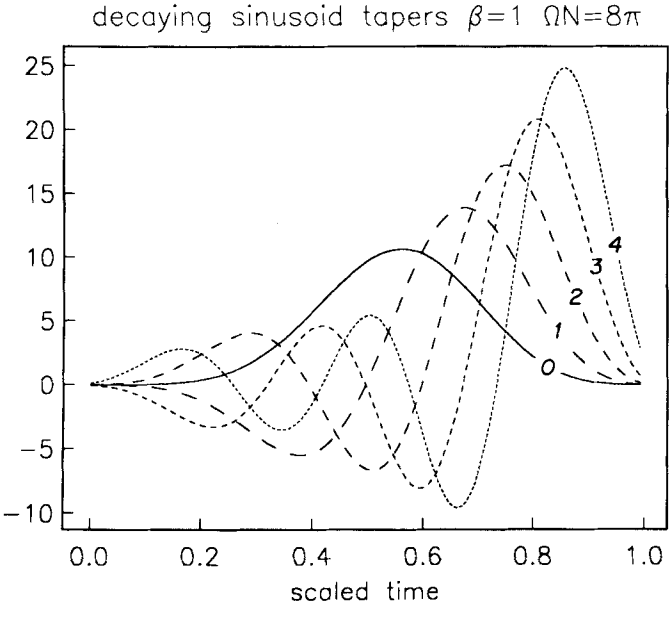

Figure 2. The five lowest-order eigentapers for a decaying sinusoid that decays by $\exp(-\pi)$ during the record. Multiplying a decaying sinusoid by these tapers will concentrate its energy in a frequency band of width $2\Omega = 16\pi/N$. The taper amplitudes increase exponentially towards the end of the record to compensate for the signal's decay.

Downloaded from https://academic.oup.com/gji/article/91/3/755/641480 by guest on 21 August 2022

unwelcome result of amplifying the late record noise as well, so that while the signal power remains constant with time in the tapered record, the noise power increases exponentially. In the next subsection we will show how noise-cognizant eigentapers weight the later data more soberly.

Substituting $\{v_t^{(k)}(N, W)\exp(\alpha t)\}_{t=0}^{N-1}$ for $\{w_k(t)\}_{t=0}^{N-1}$ in (2.5) and using the definition of λ, one can show that the discrete prolate spheroidal sequences and the sequences $\{w_k(t)\}_{t=0}^{N-1}$ have the same eigenvalues λ_k for any value of the decay rate α. Therefore, the kth prolate taper and the kth decaying sinusoid eigentaper have the same fractional spectral leakage for a given value of $P = \Omega N/2\pi$. The $2NW$ lowest-order eigenvalues λ_k of (2.6) are of order unity, and rapidly drop off thereafter (Slepian 1983). For example, 4π-prolate sequences have eight order-unity eigenvalues, one per Rayleigh frequency spacing $(2\pi/N)$ in the central region $(\hat{\omega} - 8\pi/N,\ \hat{\omega} + 8\pi/N)$. Values of λ_k are given in Table 1 for some examples of $P\pi$ prolate tapers.

The amplitudes of the frequency transforms

$$\tilde{W}_k(\omega) = \sum_{t=0}^{N-1} w_k(t)\exp(\pi\beta t/T)\exp(-i\omega t) \tag{2.8}$$

of the five lowest-order 4π-prolate eigentapers are shown in Fig. 3 over a wide range of frequencies. (Here, record length $T = N$.) Substituting $\{v_t(k)(N, W)\exp(\alpha t)\}_{t=0}^{N-1}$ for $\{w_k(t)\}_{t=0}^{N-1}$ in (2.8), one finds that the functions $\tilde{W}_k(\omega)$ are independent of decay rate. Figure 3 shows the excellent leakage rejection properties of the eigentapers. There is a sharp band-edge at frequency $\omega = 8\pi/T$. Note sidelobe height increases as the order of the taper increases, but remains 30–40 dB below the height of the central region even for the fifth taper. Figure 4 is an expansion of the central peak region displaying both real and imaginary components of the same five eigentaper transforms $\tilde{W}_k(\omega)$. The plots of the central region show that each $\tilde{W}_k(\omega)$ samples the central band $(-\Omega, \Omega)$ in a different manner. The eigentaper transforms $\tilde{W}_k(\omega)$ become increasingly more oscillatory with increasing order. The $\tilde{W}_k(\omega)$ are orthogonal, both within the central band

$$(2\pi)^{-1}\int_{-\Omega}^{\Omega} d\omega\,\tilde{W}_k^*(\omega)\,\tilde{W}_{k'}(\omega) = \mathbf{w}_k \cdot \mathbf{A} \cdot \mathbf{w}_{k'}$$

$$= \lambda_k \mathbf{w}_k \cdot \mathbf{B} \cdot \mathbf{w}_{k'} = \lambda_k \delta_{kk'} \tag{2.9}$$

Table 1. Eigenvalues λ_k for lowest-order $P\pi$ prolate tapers.

P	k	$1-\lambda_k$	P	k	$1-\lambda_k$
1	0	0.189	3	0	1.348×10^{-7}
	1	0.2504		1	9.245×10^{-6}
	2	0.7564		2	3.850×10^{-4}
				3	5.086×10^{-3}
				4	5.386×10^{-2}
2	0	5.725×10^{-5}	4	0	2.946×10^{-10}
	1	2.438×10^{-3}		1	2.768×10^{-8}
	2	4.061×10^{-2}		2	1.210×10^{-6}
	3	0.2783		3	4.245×10^{-5}
	4	0.7253		4	5.899×10^{-4}
				5	7.496×10^{-3}

Downloaded from https://academic.oup.com/gji/article/91/3/755/641480 by guest on 21 August 2022

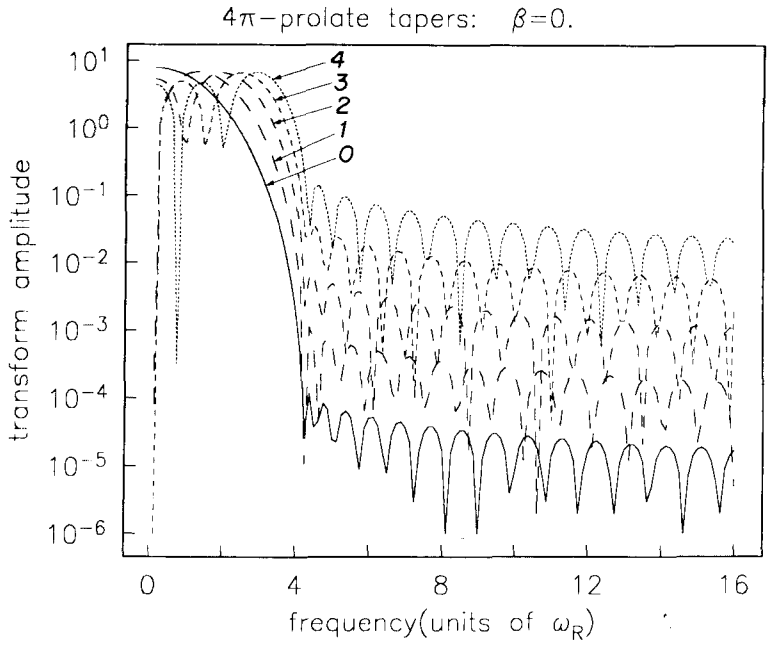

Figure 3. Frequency-transform amplitudes of the five lowest-order 4π prolate eigentapers. The frequency transforms are independent of decay rate by (2.8). The sidelobes are lowest for the optimal eigentaper, and increase in height for higher order eigentapers. The abscissa is in units of $\omega_R = 2\pi/T$, where T is the record length. There is a sharp bandedge at frequency $\omega = 4\omega_R$.

using (2.6) through (2.8), and over the entire discrete Fourier transform frequency band

$$(2\pi)^{-1} \int_{-\pi}^{\pi} d\omega \, \tilde{W}_k^*(\omega) \tilde{W}_{k'}(\omega) = \delta_{kk'} \tag{2.10}$$

by (2.7). In (2.9) and (2.10), the asterisk denotes complex conjugation.

Unfortunately, these tapers are only suitable for the analysis of noise-free records, but low frequency seismic data are noisy. In the next section, tapers designed to analyse noisy records are discussed.

2B DECAYING SIGNAL IN WHITE NOISE

Low-frequency seismic records can be modelled as a sum of decaying free oscillations immersed in noise

$$x(t) = \sum_m \mu_m \exp(i\omega_m t - \alpha_m t) + n(t); \qquad t \geqslant 0, \tag{2.11}$$

where, as before, ω_m, α_m and μ_m are the frequency, decay rate and complex amplitude of the mth free oscillation, with onset at $t = 0$, and $n(t)$ is a realization of a noise process. The sum over m extends in principle over the countably infinite elastic-gravitational free oscillations, but can be taken as finite in a record from a band-limited seismic instrument. We will assume throughout that $n(t)$ is a realization of a stationary, zero-mean, white noise process.

Downloaded from https://academic.oup.com/gji/article/91/3/755/641480 by guest on 21 August 2022

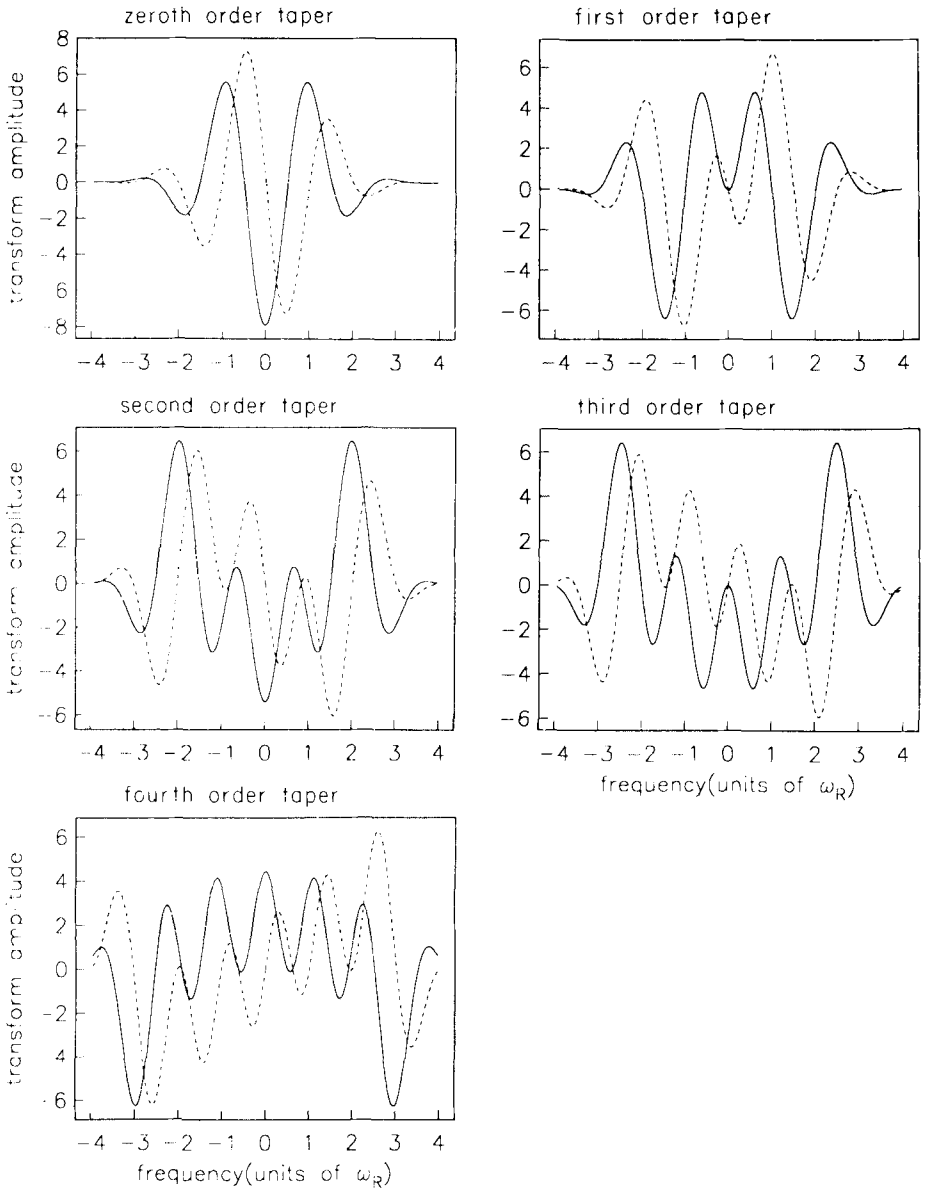

Figure 4. Expansion of central peak region of the five eigentaper frequency transforms of Fig. 3. The solid line is the real part; the dotted line is the imaginary part. The central peak region is increasingly more oscillatory for higher-order eigentapers.

In practice, the spectrum of seismic noise does not vary much over the frequency band of interest (Agnew & Berger 1978).

We determine optimal data tapers in this case using an extension of the variational formalism described above. In particular, we wish to balance the need to concentrate as much of the spectral energy of the signal as possible into a region of bandwidth 2Ω against the desire to retain a high ratio of tapered signal power to tapered noise power. The exponential asymmetry of the decaying signal tapers $\{w_k(t)\}_{t=0}^{N-1}$ will increase the

Downloaded from https://academic.oup.com/gji/article/91/3/755/641480 by guest on 21 August 2022

amplitude of stationary noise in the later part of the record. This will degrade the quality of the spectral estimate considerably unless the ratio of tapered signal to tapered noise is constrained to have a reasonable value.

Assume that in the interval $(\hat{\omega} - \Omega, \hat{\omega} + \Omega)$ the record $x(t)$ is composed of the signal, a single decaying sinusoid, plus white noise $n(t)$:

$$x(t) = \mu \exp(i\hat{\omega}t - \alpha t) + n(t). \tag{2.12}$$

Suppose also that we have discrete samples of $x(t)$

$$\{x(t)\}; \qquad t = 0, 1, 2, \ldots, N-1$$

so that the angular frequency $\omega \in (-\pi, \pi]$. We want to choose our taper $\{w(t)\}_{t=0}^{N-1}$ so that the energy of the tapered signal

$$\{w(t)\mu \exp(i\hat{\omega}t - \alpha t)\}_{t=0}^{N-1} \tag{2.13}$$

in $(\hat{\omega} - \Omega, \hat{\omega} + \Omega)$ relative to its total energy is maximized, but now with a constraint: the ratio of the tapered signal power to tapered noise power in $(\hat{\omega} - \Omega, \hat{\omega} + \Omega)$ has a fixed value.

The discrete Fourier transform of the tapered noise is

$$m(\omega) = \sum_{t=0}^{N-1} n(t) \exp(-i\omega t) w(t). \tag{2.14}$$

A measure of the expected energy of the tapered noise at frequency ω is

$$\langle |m(\omega)|^2 \rangle = \sigma_N^2 \sum_{t=0}^{N-1} [w(t)]^2, \tag{2.15}$$

where $\langle\rangle$ denotes expectation value and σ_N^2 is the noise variance. The expected power of the noise in the tapered record in $(\hat{\omega} - \Omega, \hat{\omega} + \Omega)$ is

$$\int_{\hat{\omega}-\Omega}^{\hat{\omega}+\Omega} \langle |m(\omega)|^2 \rangle d\omega = 2\Omega\sigma_N^2 \sum_{t=0}^{N-1} [w(t)]^2. \tag{2.16}$$

We generalize (2.5) in order to constrain the ratio of tapered signal to tapered noise within the frequency band $(\hat{\omega} - \Omega, \hat{\omega} + \Omega)$. We now wish to maximize the functional

$$f(\mathbf{w}; \Omega, \eta) = \frac{\mathbf{w} \cdot \mathbf{A} \cdot \mathbf{w}}{\mathbf{w} \cdot \mathbf{B} \cdot \mathbf{w}} + \eta \frac{\mathbf{w} \cdot \mathbf{A} \cdot \mathbf{w}}{\mathbf{w} \cdot \mathbf{w}} \tag{2.17}$$

with respect to $\mathbf{w}$, where $\mathbf{w}$, $\mathbf{A}$ and $\mathbf{B}$ are as defined in Section 2A. The second term in equation (2.17) represents the ratio of tapered signal power to tapered noise power; η is a Lagrange multiplier. In the limit of very large signal-to-noise ratio, i.e., as $(|\mu|^2)/(\sigma_N^2) \to \infty$, one expects η to tend to zero. In principle η is determined from the constraint equation; in practice we determine its value empirically. The condition $\delta f(\mathbf{w}; \Omega, \eta) = 0$ leads to a non-linear equation for the tapers $\mathbf{w}$ which maximize (2.17). This non-linear equation can be solved approximately (Lindberg 1986).

Alternatively, we can minimize the functional

$$\tilde{f}(\mathbf{w}; \Omega, \nu) = \frac{\mathbf{w} \cdot \mathbf{B} \cdot \mathbf{w}}{\mathbf{w} \cdot \mathbf{A} \cdot \mathbf{w}} + \nu \frac{\mathbf{w} \cdot \mathbf{w}}{\mathbf{w} \cdot \mathbf{A} \cdot \mathbf{w}} \tag{2.18}$$

Downloaded from https://academic.oup.com/gji/article/91/3/755/641480 by guest on 21 August 2022

(F. Gilbert, private communcation). Solving $\delta\tilde{f} = 0$ leads to the equation

$$\mathbf{A} \cdot \mathbf{w} = \lambda' \mathbf{B}' \cdot \mathbf{w}, \tag{2.19}$$

where $\mathbf{B}' = \mathbf{B} + \nu\mathbf{I}$, $\mathbf{I}$ being the $N \times N$ identity matrix and

$$\lambda' = [\tilde{f}(\mathbf{w}; \Omega, \nu)]^{-1}.$$

The eigenvectors which correspond to the largest eigenvalues λ' of (2.19) will minimize $\tilde{f}$.

Given the decay rate α and the noise-weighting parameter ν, (2.19) can be solved for eigentapers $\{w_k(t; \beta, \nu)\}_{t=0}^{N-1}$. When $\nu = 0$, the elements of the kth taper $w_k(t; \beta, 0) = w_k(t)$; $t = 0, 2, \ldots, N-1$, and the tapers reduce to those of Section 2A. The fraction of tapered signal power that remains in the frequency band $(\hat{\omega} - \Omega, \hat{\omega} + \Omega)$ is

$$(\mathbf{w}_k \cdot \mathbf{A} \cdot \mathbf{w}_k)/(\mathbf{w}_k \cdot \mathbf{B} \cdot \mathbf{w}_k) = \lambda_k \tag{2.20}$$

which can be calculated from the eigenvectors and eigenvalues of (2.19). We have found it helpful to think of the λ_k as 'bandwidth retention factors'.

We used EISPACK subroutines (Smith *et al.* 1976) to solve (2.19) for its largest eigenvalues λ_k' and associated eigenvectors. We normalized the tapers $\{w_k(t; \beta, \nu)\}_{t=0}^{N-1}$ so that

$$\mathbf{w}_k \cdot \mathbf{B}' \cdot \mathbf{w}_{k'} = \sum_{t=0}^{N-1} (\exp(-2\alpha t) + \nu)\, \mathbf{w}_k(t; \beta, \nu)\, \mathbf{w}_{k'}(t; \beta, \nu) = \delta_{kk'}. \tag{2.21}$$

Rather than solve an eigenvalue problem for every data series length, (2.19) was solved for $N = 128$ and the tapers for other values of N were found using spline interpolation. This approach takes advantage of the asymptotic relations between the discrete and continuous-time tapers described in Slepian (1978). Tests using these interpolated tapers showed negligible degradation of spectral leakage properties relative to exact solutions for $N > 128$. For $N \ll 128$, (2.19) should be solved directly (A. Chave, private communication), but such short time series are rare in free oscillation work. The taper transforms are computed from the interpolated tapers using an FFT after padding the tapers with zeroes until their lengths were a power of two.

The preceding argument shows that ν is a complicated function of the signal-to-noise ratio. For large signal-to-noise-ratios $|\mu|^2/\sigma_N^2$, ν will be very small, $\mathbf{B}' \approx \mathbf{B}$, and the solution of (2.19) is not very different from the solution of (2.6). For smaller signal-to-noise ratios, one expects that the optimal tapers will have a ν of finite size. One could pick an incorrect value of ν for a particular signal-to-noise ratio, but then the tapers would not perform optimally. Useful values are best determined by experiment. We will show in the appendix that using eigentapers having larger values of ν results in a marked improvement in the detection capability of the multiple-taper algorithm.

Some examples of noise-cognizant eigentapers are exhibited in Fig. 5 for the case $\nu = 0.01$, $\beta = 0.6$, and $\Omega N = 8\pi$. Note the strong asymmetry of the tapers, with a strong emphasis on data in the earlier section of the record where instantaneous signal-to-noise ratio is greater. The height of the taper's main peak increases with increasing order to compensate for the decay of the signal, as shown in Fig. 2. Figure 6 shows tapers which were designed with $\nu = 0.1$, $\beta = 0.6$, and $\Omega N = 8\pi$. The preference for the early part of the record is more drastic, resulting in significant weighting at the onset of the time series. Here the variational principle minimizing (2.18) has sacrificed resistance to spectral leakage in order to raise the ratio of tapered signal to tapered noise. Figure 7 displays eigentapers designed with $\nu = 0.001$, $\beta = 0.2$, and $\Omega N = 8\pi$. These eigentapers are for a series containing sinusoids that only decay slightly in a more favourable signal-to-noise environment. Asymmetrical weighting remains

Downloaded from https://academic.oup.com/gji/article/91/3/755/641480 by guest on 21 August 2022

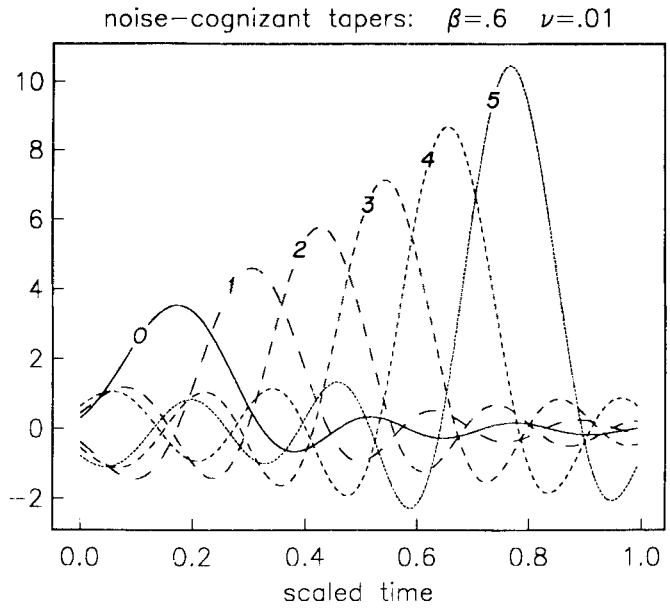

Figure 5. Optimal eigentapers for an exponentially decaying sinusoid immersed in white noise. The sinusoid is assumed to decay by exp (-0.6π) during the record. The noise parameter ν is chosen according to the signal-to-noise ratio of the data. The tapers sample the front of the record where the signal-to-noise ratio is largest, and increase in amplitude towards the end of the record to compensate for the signal's decay.

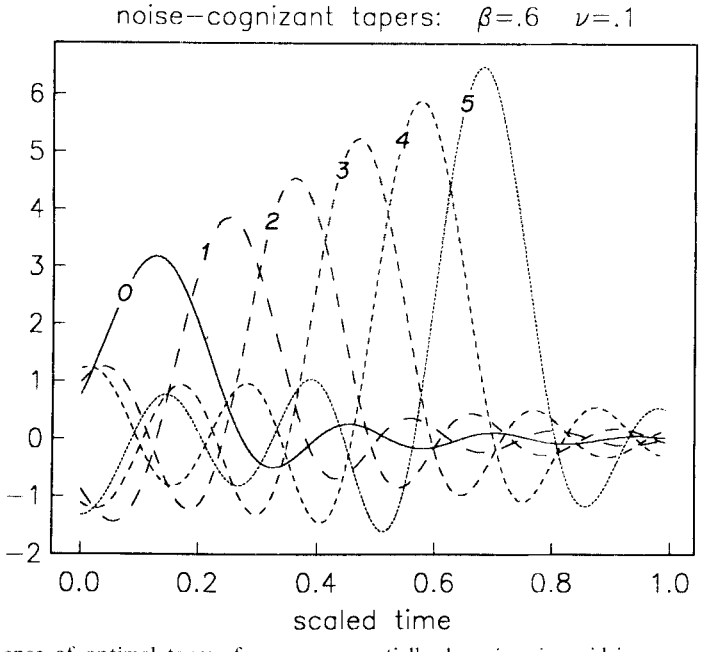

Figure 6. Sequence of optimal tapers for an exponentially decaying sinusoid immersed in white noise. These tapers are designed for a lower signal-to-noise ratio than those of Fig. 5, and have a larger noise parameter ν. These tapers sample the data less heavily in the latter part of the record where the signal is obscured by noise, compared to the tapers in Fig. 5.

Downloaded from https://academic.oup.com/gji/article/91/3/755/641480 by guest on 21 August 2022

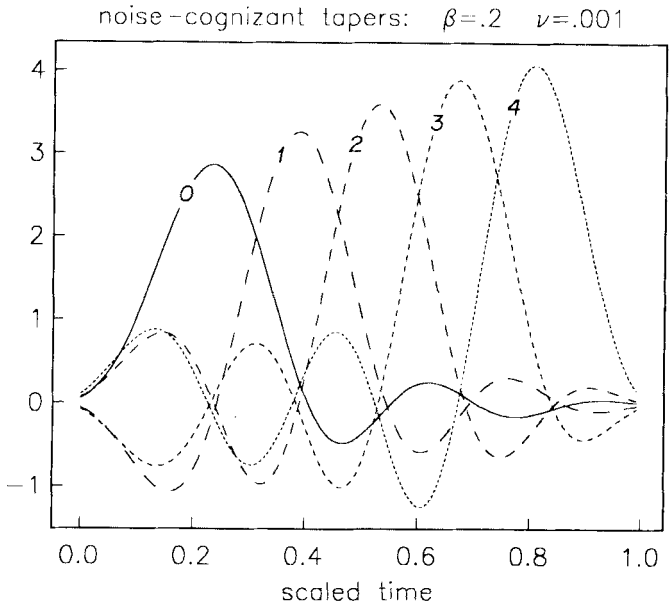

Figure 7. Set of optimal eigentapers for a decaying sinusoid contaminated by additive white noise. Compared with the tapers if Figs 5 and 6, these eigentapers are designed for records with a larger signal-to-noise ratio, and a sinusoid that decays less.

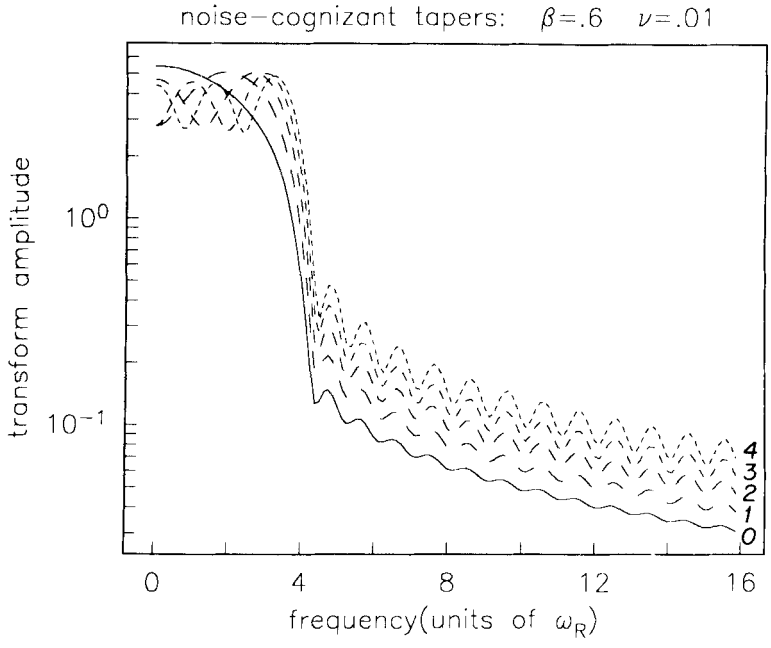

Figure 8. Amplitude of the five lowest-order noise-cognizant eigentapers with decay parameter $\beta = 0.6$, noise parameter $\nu = 0.01$ and time-bandwidth product $N\Omega = 8\pi$. The abscissa is in units of $\omega_R = 2\pi/T$. There is a sharp bandedge at frequency $\omega = 4\omega_R = 8\pi/T$. Note that the plot is of absolute magnitude, not power, so the first sidelobes are 20–30 dB down.

Downloaded from https://academic.oup.com/gji/article/91/3/755/641480 by guest on 21 August 2022

Table 2. Eigenvalues λ_k' and bandwidth retention factors λ_k for lowest order noise-cognizant optimal tapers.

	$\nu=0.01, \beta=0.6$		$\nu=0.1, \beta=0.6$		$\nu=0.001, \beta=0.2$		$\nu=0.01, \beta=1$	
k	λ_k'	λ_k	λ_k'	λ_k	λ_k'	λ_k	λ_k'	λ_k
0	0.962301	0.99869	0.73574	0.98905	0.99729	0.99997	0.94592	0.99682
1	0.940787	0.99760	0.63985	0.98003	0.99676	0.99995	0.89435	0.99227
2	0.910363	0.99619	0.53070	0.96888	0.99614	0.99993	0.80953	0.98428
3	0.867487	0.99361	0.41590	0.95026	0.99542	0.99990	0.68406	0.96699
4	0.808944	0.99006	0.30618	0.92719	0.99458	0.99975	0.52440	0.93826
5	0.732283	0.98339	0.21152	0.89053	0.98934	0.99469	0.35619	0.88398

Values of the eigenvalues λ_k' and the bandwidth retention factors λ_k for time-bandwidth product $\Omega N = 8\pi$ and various values of the decay parameter β and the noise parameter ν. Note that the bandwidth retention parameters λ_k are close to 1 for small k, and are succeedingly smaller for higher order tapers. The lowest order eigentapers have the smallest fractional leakage $1-\lambda_k$; higher order eigentapers suffer from successively greater spectral leakage.

evident. Table 2 shows values of λ_k' and λ_k for tapers $\{w_k(t;\beta,\nu)\}_{t=0}^{N-1}$ for a selection of β and ν values. The eigenvalues λ_k' drop rapidly from unity with increasing k. The bandwidth retention factors λ_k remain relatively constant among eigentapers of fixed β and ν. This behaviour can be observed qualitatively in the Fig. 8 plots of the amplitudes of the frequency transforms $\tilde{W}_k(w;\beta,\nu)$ of the tapers $\{w_k(t;\beta,\nu)\}_{t=0}^{N-1}$

$$\tilde{W}_k(\omega;\beta,\nu) = \sum_{t=0}^{N-1} w_k(t;\beta,\nu) \exp\left[(-\pi\beta/T)\,t\right] \exp(-i\omega t) \tag{2.22}$$

for $\beta = 0.6$, $\nu = 0.01$, and $\Omega N = 8\pi$. The five lowest order eigentapers have sidelobes of comparable height. Enlargements of the central peak regions are shown in Fig. 9.

Because **A** and **B**′ are symmetric, the orthogonality condition (2.9) remains valid for noise-cognizant tapers, using (2.21). However, as the noise-cognizant tapers $\{w_k(t;\beta,\nu)\}_{t=0}^{N-1}$ satisfy (2.21) and not (2.7), the frequency-domain orthogonality relation (2.10) does not

Table 3. Elements of matrix **D** for $\beta = 0.6$, $\Omega N = 8\pi$ and $\nu = 0.01$.

	k'				
k	0	1	2	3	4
0	0.98151	−0.00183	0.00218	−0.00235	0.00227
1	−0.00183	0.97130	−0.00352	0.00415	−0.00445
2	0.00218	−0.00352	0.95658	−0.00620	0.00719
3	−0.00235	0.00415	−0.00620	0.93560	−0.01043
4	0.00227	−0.00445	0.00719	−0.01043	0.90638

for $\beta = 0.6$, $\Omega N = 8\pi$, and $\nu = 0.1$

	k'				
k	0	1	2	3	4
0	0.86278	−0.01271	−0.01358	0.01261	0.00995
1	−0.01271	0.80917	0.02210	−0.02322	−0.02143
2	−0.01358	0.02210	0.74322	−0.03364	−0.03440
3	0.01261	−0.02322	−0.03364	0.66634	0.04693
4	0.00995	−0.02143	−0.03440	0.04693	0.58231

Downloaded from https://academic.oup.com/gji/article/91/3/755/641480 by guest on 21 August 2022

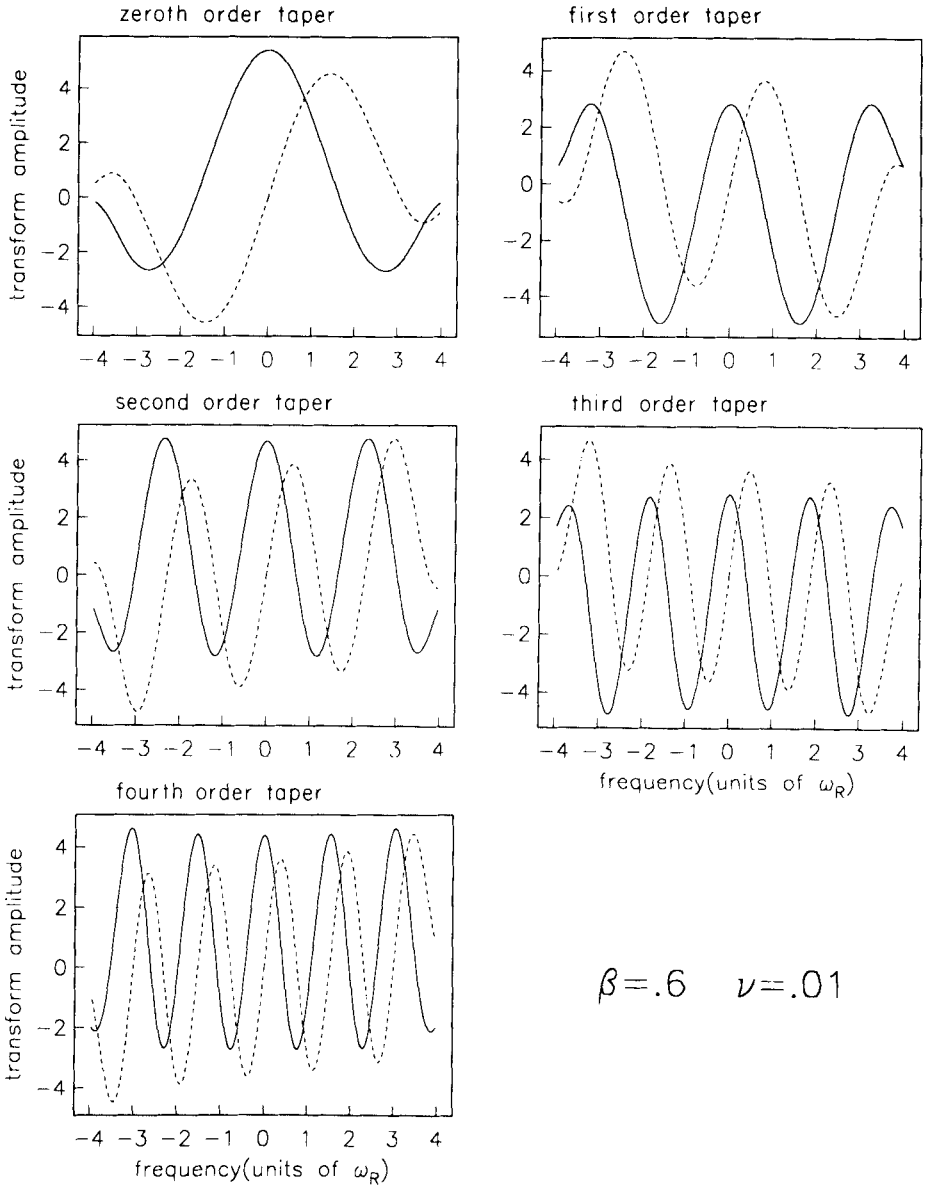

Figure 9. Expansion of the central peak region of the frequency transform amplitudes of the five lowest order eigentapers of Fig. 8. The solid line is the real part of the frequency transform; the dashed line is the imaginary part of the transform.

hold. In its place we have

$$(2\pi)^{-1}\int_{-\pi}^{\pi} d\omega \tilde{W}_k^*(\omega;\beta,\nu)\,\tilde{W}_{k'}(\omega;\beta,\nu) = \sum_{t=0}^{N-1} \exp\left[(-2\pi\beta/T)t\right] w_k(t;\beta,\nu)\, w_{k'}(t;\beta,\nu) = D_{kk'} \tag{2.23}$$

for $k, k' \epsilon \{0, 1, \ldots, K-1\}$. The matrix $\mathbf{D}$ is diagonally dominant for small ν. Table 3 lists the elements of $\mathbf{D}$ for the five lowest order eigentapers with $\Omega N = 8\pi$, $\beta = 0.6$, and $\nu = 0.01$

Downloaded from https://academic.oup.com/gji/article/91/3/755/641480 by guest on 21 August 2022

or $\nu = 0.1$. The magnitude of the off-diagonal elements of **D** indicate the departure from orthogonality of the frequency transforms $\widetilde{W}_k(\omega; \beta, \nu)$ over $(-\pi, \pi]$.

We have required that our data tapers possess certain desirable properties. We want them to have the ability to concentrate most of a decaying sinusoid's energy into a given frequency band, balanced against the capacity to maintain a high signal-to-noise ratio for the tapered data in the frequency domain. This leads to a variational calculus problem, whose solutions are a family of data tapers. These tapers provide a method of orthogonally sampling a decaying sinusoid, in both the time and frequency domains. By sampling a decaying sinusoid repeatedly in different ways, one can obtain superior estimates of its frequency and amplitude. Simple techniques to do this, based on those outlined by Thomson (1982), are the subject of the next section.

3 Harmonic analysis

An important part of long-period seismic data analysis is the detection of decaying sinusoids in the data and the measurement of their frequencies and amplitudes. The estimation of decay rate α is also important; we plan to address this problem in later work. In the following it is assumed that the Q of the decaying oscillation is known or has been approximated by some method (e.g. Riedesel *et al.* 1980).

The spectra of low-frequency seismic time-series consist of harmonic 'lines' which have been broadened by decay, and a continuous background spectrum. The decay-broadened 'lines' are treated as signal, whereas the continuous spectrum is considered to be noise. This sets free oscillation data analysis apart from many familiar problems in seismic spectral estimation, e.g. finding the frequency content of body waves, or earthquakes in the near field. The spectra in those cases are predominantly continuous. There are methods of multitaper spectrum analysis that are useful for spectra which do not have harmonic line components (e.g. Thompson 1982; Park, Lindberg & Vernon, in press; Lindberg, Vernon & Park, unpublished manuscript).

The most straightforward method of detecting line components in low-frequency data is to measure obvious spectral peaks in a discrete Fourier transform of the data. If one tapers the time series in a prudent fashion, as indicated in Dahlen (1982), this approach is adequate for well-excited oscillations generated by large earthquakes ($M_L \gtrsim 7$). Unfortunately, most of these well-excited oscillations are surface-wave-equivalent fundamental modes which by themselves allow poor depth resolution. The modes most useful for enhancing the resolution at depth (e.g. the overtone oscillations that correspond to *PKP, PKIKP, SKS* etc. motion) are excited only by very large or very deep earthquake sources. Even then, their spectral peaks may not protrude substantially above the background noise. Masters & Gilbert (1981) show a typical example of this problem in the presumed identification of two inner-core oscillations. The use of spherical harmonic stacking of records from a global array (Gilbert & Backus 1965; Gilbert & Dziewonski 1975; Buland, Berger & Gilbert 1979) can aid mode identification greatly, especially in the case of closely spaced spectral lines caused by splitting of a free oscillation into individual singlets. However, it is difficult to identify decaying sinusoids in a low signal-to-noise environment using conventional methods of spectral estimation.

In the following we propose a method that is designed to yield a quantitative measure of the certainty that there is a decaying sinusoid at any given frequency. The novelty of our algorithm resides in the additional information obtained by sampling the data with more than one taper and the introduction of a statistical theory based on an F-test to detect harmonic spectral components and reject continuous, random-phase noise.

Downloaded from https://academic.oup.com/gji/article/91/3/755/641480 by guest on 21 August 2022

3.1 REGRESSION ANALYSIS

Suppose that $x(t)$ is a record consisting of noise and a number of decaying sinusoids, one of which has frequency $\hat{\omega}$. Then one can write

$$x(t) = \mu \exp(i\hat{\omega}t - \alpha t) + e(t), \tag{3.1}$$

where μ is a complex amplitude, α is a decay rate, and $e(t)$ is an error term. The error term consists of other decaying sinusoids and noise. For a sufficiently small value of Ω, $x(t)$ contains only the single decaying sinusoid $\mu \exp(i\hat{\omega}t - \alpha t)$ in the frequency interval $(\hat{\omega} - \Omega, \hat{\omega} + \Omega)$. This decaying sinusoid represents a deterministic signal in the record $x(t)$, and one can use the method of least squares to estimate its amplitude μ.

We assume in the following that there is not more than one decaying sinusoid in the frequency interval $(\hat{\omega} - \Omega, \hat{\omega} + \Omega)$. This is often not true in practice, but in many applications the various singlets of free oscillation multiplets are observed to combine into a signal that is well approximated by a single resonance. Also, the least-squares procedure can be generalized to the case of two or more decaying sinusoids in a frequency interval of width 2Ω (Thomson 1982).

As we have indicated, it is important to taper the data. Using the optimal tapers of Section 2, we multiply the data by each taper $\{w_k(t;\beta,\nu)\}_{t=0}^{N-1}$, $k = 0, 1, 2, \ldots, K-1$, in turn. We pick only a small number (K) of data tapers because higher order tapers have successively poorer leakage resistance. In the case $\nu = 0$ the tapers up to order $K = N \cdot \Omega/\pi$ have good spectral leakage resistance; higher-order tapers exhibit vastly poorer performance (Slepian 1978). This is evident from the behaviour of the eigenvalues λ_k appearing in Table 1. In the case $\nu \neq 0$, we choose the K noise-cognizant tapers with the largest bandwidth retention factors. Usually $K < N\Omega/\pi$ in this case. We show how we choose K in Section 4.

Multiplying the data $\{x(t)\}_{t=0}^{N-1}$ by the K eigentapers $\{w_k(t;\beta,\nu)\}_{t=0}^{N-1}$ one obtains K time series:

$$\{w_k(t;\beta,\nu)x(t)\}_{t=0}^{N-1};\ k = 0, 1, \ldots, K-1.$$

From equation (3.1)

$$e(t)w_k(t;\beta,\nu) = x(t)w_k(t;\beta,\nu) - \mu w_k(t;\beta,\nu)\exp(i\hat{\omega}t - \alpha t); \qquad t = 0, 1, \ldots, N-1. \tag{3.2}$$

Take the discrete Fourier transform of both sides of (3.2):

$$e_k(\omega) = y_k(\omega) - \mu \tilde{W}_k(\omega - \hat{\omega};\beta,\nu), \tag{3.3}$$

where

$$e_k(\omega) = \sum_{t=0}^{N-1} e(t)\omega_k(t;\beta,\nu)\exp(-i\omega t)$$

$$y_k(\omega) = \sum_{t=0}^{N-1} x(t)w_k(t;\beta,\nu)\exp(-i\omega t)$$

and $\tilde{W}_k(\omega;\beta,\nu)$ is defined in equation (2.22). Because of the leakage resistance of the tapers, the $e_k(\omega)$ are approximately the complex eigenspectra of the noise in $(\hat{\omega} - \Omega, \hat{\omega} + \Omega)$.

We would like to make an estimate $\hat{\mu}$ of the amplitude μ of a decaying sinusoid of frequency $\hat{\omega}$. To do this, a least-squares procedure is performed. At each frequency ω, the complex eigenspectra $y_k(\omega)$, $k = 0, 1, \ldots, K-1$, are taken to be the dependent variables,

Downloaded from https://academic.oup.com/gji/article/91/3/755/641480 by guest on 21 August 2022

$\hat{\mu}$ is the parameter to be estimated, and the $\widetilde{W}_k(\omega - \hat{\omega}; \beta, \nu)$, $k = 0, 1, \ldots, K-1$, are the independent variables. By the Gauss–Markov theorem, to produce a minimum variance estimate of μ that is unbiased at the decaying sinusoid's true frequency using least squares, the random variables $y_k(\omega)$ must be statistically uncorrelated (Bickel & Doksum 1977, ch. 7; Luenberger 1969, ch. 4; Tukey 1975). However, the $y_k(\omega)$ are not necessarily uncorrelated random variables:

$$\text{Cov}\,[y_k(\omega), y_{k'}(\omega)] = \langle y_k(\omega)\, y_{k'}^*(\omega)\rangle - \langle y_k(\omega)\rangle \langle y_{k'}(\omega)\rangle^*$$

$$= \sigma_N^2 \sum_{t=0}^{N-1} w_k(t; \beta, \nu)\, w_{k'}(t; \beta, \nu). \tag{3.4}$$

The sum

$$H_{kk'} = \sum_{t=0}^{N-1} w_k(t; \beta, \nu)\, w_{k'}(t; \beta, \nu)$$

will not vanish unless $\beta = \nu = 0$ and $k \neq k'$. For $\beta = \nu = 0$, $H_{kk'} = \delta_{kk'}$. Elements of the matrix **H** for $\beta = 0.6$, $\Omega N = 8\pi$, and $\nu = 0.01$ and $\nu = 0.1$ are shown in Table 4.

Since **H** is symmetric and positive definite, it has a Cholesky decomposition. That is, there exists a lower triangular matrix **G** with positive diagonal entries such that

$$\mathbf{H} = \mathbf{G}\mathbf{G}^T \tag{3.5}$$

where the superscript T denotes matrix transpose (Golub & VanLoan 1983).

Transform the complex eigenspectra $y_k(\omega)$ and the independent variables $\widetilde{W}_k(\omega; \beta, \nu)$ using the matrix $\mathbf{G}^{-1}$ as follows:

$$\begin{aligned} v_{k'}(t; \beta, \nu) &= (\mathbf{G}^{-1})_{k'k}\, w_k(t; \beta, \nu) \\ z_{k'}(\omega) &= (\mathbf{G}^{-1})_{k'k}\, y_k(\omega) \\ V_{k'}(\omega_j; \beta, \nu) &= (\mathbf{G}^{-1})_{k'k}\, \widetilde{W}_k(\omega_j; \beta, \nu) \\ g_{k'}(\omega) &= (\mathbf{G}^{-1})_{k'k}\, e_k(\omega), \end{aligned} \tag{3.6}$$

Table 4. Elements of matrix **H** for $\beta = 0.6$, $\Omega N = 8\pi$ and $\nu = 0.01$.

	k'				
k	0	1	2	3	4
0	1.84870	0.18322	−0.21788	0.23523	−0.22668
1	0.18322	2.86999	0.35164	−0.41490	0.44470
2	−0.21788	0.35164	4.34203	0.61999	−0.71893
3	0.23523	−0.41490	0.61999	6.44037	1.04331
4	−0.22668	0.44470	−0.71893	1.04331	9.36201

for $\beta = 0.6$, $\Omega N = 8\pi$, and $\nu = 0.1$

	k'				
k	0	1	2	3	4
0	1.37223	0.12714	0.13583	−0.12606	−0.09953
1	0.12714	1.90834	−0.22102	0.23223	0.21434
2	0.13583	−0.22102	2.56776	0.33639	0.34401
3	−0.12606	0.23223	0.33639	3.33664	−0.46931
4	−0.09953	0.21434	0.34401	−0.46931	4.17692

Downloaded from https://academic.oup.com/gji/article/91/3/755/641480 by guest on 21 August 2022

where $v_k(t;\beta,\nu)$, $z_k(\omega_j)$, $V_k(\omega_j;\beta,\nu)$ and $g_{k'}(\omega_j)$ are the transformed tapers, the transformed complex eigenspectra, the transformed independent variables, and the transformed errors respectively. We employ the Einstein summation convention in (3.6) and hereafter, summing repeated indices over the range $0, 1, \ldots, K-1$. From (3.3),

$$g_k(\omega) = z_k(\omega) - \hat{\mu} V_k(\omega - \hat{\omega};\beta,\nu). \tag{3.7}$$

The transformed complex eigenspectra $z_k(\omega)$ are uncorrelated, as

$$\begin{aligned}\mathrm{Cov}\,[z_k(\omega), z_{k'}(\omega)] &= \langle z_k(\omega) z_{k'}^*(\omega)\rangle - \langle z_k(\omega)\rangle\langle z_{k'}(\omega)\rangle^* \\ &= (\mathbf{G}^{-1})_{kl}\,\mathrm{Cov}\,[y_l(\omega), y_m(\omega)]\,(\mathbf{G}^{-1})_{k'm} \\ &= \sigma_N^2 \delta_{kk'}\end{aligned} \tag{3.8}$$

by (3.4) and (3.5).

A measure of the error in assuming that the record $x(t)$ consists of a single decaying sinusoid of frequency $\hat{\omega}$ is

$$M(\omega) = \sum_{k=0}^{K-1} |g_k(\omega)|^2 = \sum_{k=0}^{K-1} |z_k(\omega) - \hat{\mu} V_k(\omega - \hat{\omega};\beta,\nu)|^2. \tag{3.9}$$

Perform a least squares procedure; solve

$$\frac{\partial M(\omega)}{\partial \hat{\mu}^*} = 0 \tag{3.10}$$

for $\hat{\mu}$. Then (3.10) becomes

$$0 = \sum_{k=0}^{K-1} V_k^*(\omega - \hat{\omega};\beta,\nu)\,[z_k(\omega) - \mu V_k(\omega - \hat{\omega};\beta,\nu)]. \tag{3.11}$$

Note that $\hat{\mu}$ is actually a function of the frequency $\hat{\omega}$:

$$\hat{\mu} = \hat{\mu}(\hat{\omega}) = \frac{\sum_{k=0}^{K-1} V_k^*(\omega - \hat{\omega};\beta,\nu)\, z_k(\omega)}{\sum_{k=0}^{K-1} |V_k(\omega - \hat{\omega};\beta,\nu)|^2}. \tag{3.12}$$

One can determine $z_k(\omega)$ at a set of discrete frequencies $\omega_j; j = 0, 1, 2, \ldots, J-1$, called bin frequencies, by applying an FFT to the tapered data. The data can be padded with zeroes to interpolate the spectrum. (Note that this 'interpolation' adds no extra information.) To estimate the amplitude $\hat{\mu}$ of the proposed signal at each discrete bin frequency, set $\omega = \hat{\omega} = \omega_j; j = 0, 1, \ldots, J-1$ in (3.12). Then

$$\hat{\mu}(\omega_j) = \frac{\sum_{k=0}^{K-1} V_k^*(0;\beta,\nu)\, z_k(\omega_j)}{\sum_{k=0}^{K-1} |V_k(0;\beta,\nu)|^2}. \tag{3.13}$$

Downloaded from https://academic.oup.com/gji/article/91/3/755/641480 by guest on 21 August 2022

Substituting for $z_k(\omega)$ in (3.13), it is seen that this 'pointwise regression' formula for $\hat{\mu}$ is equivalent to a Fourier transform of the time series $\{x(t)\}_{t=0}^{N-1}$ with a hybrid taper $\{\hat{w}(t;\beta,\nu)\}_{t=0}^{N-1}$ given by the formula

$$\hat{w}(t;\beta,\nu) = \frac{\sum_{k=0}^{K-1} V_k(0;\beta,\nu)\, v_k(t;\beta,\nu)}{\sum_{k=0}^{K-1} |V_k(0;\beta,\nu)|^2}; \qquad t = 0, 1, \ldots, N-1 \tag{3.14}$$

($V_k^*(0;\beta,\nu) = V_k(0;\beta,\nu)$ since $\{w_k(t;\beta,\nu)\}_{t=0}^{N-1}$ is a real-valued sequence.) Note that $\{\hat{w}(t;\beta,\nu)\}_{t=0}^{N-1}$ is not optimal in the sense of (2.19).

In terms of the complex eigenspectra and taper frequency transforms:

$$\hat{\mu}(\omega_j) = \frac{\sum_{m=0}^{K-1}\sum_{l=0}^{K-1} \tilde{W}_m^*(0;\beta,\nu)(\mathbf{H}^{-1})_{ml} y_l(\omega_j)}{\sum_{m=0}^{K-1}\sum_{l=0}^{K-1} \tilde{W}_m^*(0;\beta,\nu)(\mathbf{H}^{-1})_{ml}\tilde{W}_l(0;\beta,\nu)}. \tag{3.15}$$

When $\beta = \nu = 0$, $\mathbf{H} = \mathbf{I}$, and (3.15) reduces to equation (13.5) of Thomson (1982).

If $\nu = 0$ (i.e. tapers designed without provision for stationary background noise) or $\beta = 0$ (tapers designed for non-decaying signals), $\tilde{W}_k(0;\nu,0) = \tilde{W}_k(0;0,\beta) = 0$ for odd k, since in both cases the $\tilde{W}_k$ reduce to the transforms of discrete prolate spheroidal sequences. In these instances the pointwise regression technique ignores the odd order tapers completely in constructing $\hat{\mu}$.

By (3.8),

$$\begin{aligned}\mathrm{Var}\,[\hat{\mu}(\omega_j)] &= \frac{\sum_{k=0}^{K-1} |V_k(0;\beta,\nu)|^2 \mathrm{Var}\,[z_k(\omega_j)]}{\left(\sum_{k=0}^{K-1} |V_k(0;\beta,\nu)|^2\right)^2} \\ &= \frac{\sigma_N^2}{\sum_{m=0}^{K-1}\sum_{l=0}^{K-1} \tilde{W}_m^*(0;\beta,\nu)(\mathbf{H}^{-1})_{ml}\tilde{W}_l(0;\beta,\nu)}.\end{aligned} \tag{3.16}$$

The variance of the estimated amplitude increases with increasing noise amplitude.

If there is no decaying sinusoid at frequency ω_j, one would expect $\hat{\mu}$ to be small. However, this is not the best criterion for deciding if there is a decaying sinusoid at frequency ω_j. The sinusoid may be present, but it may have a very small amplitude. Also, the least squares procedure may yield a large value for $\hat{\mu}$ at some frequency, but a decaying sinusoid may not be a good way to characterize the data at that frequency. A method of evaluating the fit of our decaying sinusoid model to the data is needed.

3.2 TESTING THE FIT OF THE MODEL TO THE DATA

A common technique for assessing the fit of a least-squares estimate is to perform a statistical

Downloaded from https://academic.oup.com/gji/article/91/3/755/641480 by guest on 21 August 2022

F-test (e.g. Wonnacott & Wonnacott 1981). An F-statistic is roughly the ratio

$$F = \frac{\text{variance explained by the model}}{\text{unexplained variance}}. \tag{3.17}$$

The random variable F follows the F-distribution, which has been tabulated (e.g. Abramowitz & Stegun 1965). We use the F-test to compare the fit of the data to a decaying sinusoid model.

Suppose that the record $x(t)$ consists *solely* of zero-mean stationary Gaussian white noise $n(t)$. For free oscillation data, we have found that it is a reasonable approximation to say the background noise is Gaussian white noise and almost stationary. This can be demonstrated by generating ordered value plots of the data, as in Fig. 10 [Wilk & Gnanadesiken (1968) contains details on ordered value, or $P-P$ plotting of data].

As before, one estimates the complex amplitude μ of a decaying sinusoid of frequency $\hat{\omega}$ by fitting the model $\hat{\mu}\,\tilde{W}_k(\omega - \hat{\omega}; \beta, \nu)$ to the random variables

$$y_k(\omega) = \sum_{t=0}^{N-1} w_k(t; \beta, \nu) \exp(-i\omega t)\, n(t); \qquad k = 0, 1, \ldots, K-1. \tag{3.18}$$

There is a finite probability that a decaying sinusoid model will fit the complex eigenspectra of the noise (3.18) at some frequency. The chance that this will happen is a measure of the confidence that a true decaying sinusoid exists at that frequency.

When no harmonic signal is present, the expected value of each transformed complex eigenspectrum vanishes:

$$\langle z_k(\omega_j) \rangle = 0. \tag{3.19}$$

However, the presence of noise, or signal, may cause any given transformed complex eigenspectrum $z_k(\omega_j)$ to be non-zero at some frequencies. This departure of $z_k(\omega_j)$ from its expected value may be partly 'explained' by the linear regression analysis. Using the estimated value $\hat{\mu}\ (\omega_j)$ from (3.13), the estimated value of $z_k(\omega_j)$ is

$$\hat{z}_k(\omega_j) = \hat{\mu}(\omega_j)\, V_k(0; \beta, \nu). \tag{3.20}$$

The deviation of $z_k(\omega_j)$ from $\langle z_k(\omega_j) \rangle$ may be decomposed into an 'explained' deviation, $[\hat{z}_k(\omega_j) - \langle z_k(\omega_j) \rangle]$ and an 'unexplained' deviation, $[z_k(\omega_j) - \hat{z}_k(\omega_j)]$:

$$[z_k(\omega_j) - \langle z_k(\omega_j) \rangle] = [\hat{z}_k(\omega_j) - \langle z_k(\omega_j) \rangle] + [z_k(\omega_j) - \hat{z}_k(\omega_j)]. \tag{3.21}$$

Or, summing over k, and noting that $\langle z_k(\omega_j) \rangle = 0$

$$\sum_{k=0}^{K-1} z_k(\omega_j) = \sum_{k=0}^{K-1} \hat{z}_k(\omega_j) + \sum_{k=0}^{K-1} [z_k(\omega_j) - \hat{z}_k(\omega_j)]. \tag{3.22}$$

The same equality holds when one takes the modulus squared of the deviations:

$$\sum_{k=0}^{K-1} |z_k(\omega_j)|^2 = \sum_{k=0}^{K-1} |\hat{z}_k(\omega_j)|^2 + \sum_{k=0}^{K-1} |z_k(\omega_j) - \hat{z}_k(\omega_j)|^2 \tag{3.23}$$

by multiplying (3.21) by its complex conjugate, and then summing over k. Substituting for $\hat{z}_k(\omega_j)$, (3.23) becomes

$$\sum_{k=0}^{K-1} |z_k(\omega_j)|^2 = |\hat{\mu}(\omega_j)|^2 \sum_{k=0}^{K-1} |V_k(0; \beta, \nu)|^2 + \sum_{k=0}^{K-1} |z_k(\omega_j) - \hat{\mu}(\omega_j)\, V_k(0; \beta, \nu)|^2 \tag{3.24}$$

Downloaded from https://academic.oup.com/gji/article/91/3/755/641480 by guest on 21 August 2022

or

$$\xi(\omega_j) = \theta(\omega_j) + \psi(\omega_j), \tag{3.25}$$

defining

$$\xi(\omega_j) \equiv \sum_{k=0}^{K-1} |z_k(\omega_j)|^2$$

$$\theta(\omega_j) \equiv |\hat{\mu}(\omega_j)|^2 \sum_{k=0}^{K-1} |V_k(0;\beta,\nu)|^2$$

$$\psi(\omega_j) \equiv \sum_{k=0}^{K-1} |z_k(\omega_j) - \hat{\mu}(\omega_j) V_k(0;\beta,\nu)|^2,$$

where $\xi(\omega_j)$ is the total sample variance of the $z_k(\omega_j)$, $\theta(\omega_j)$ is the sample variance explained by the decaying sinusoid hypothesis, and $\psi(\omega_j)$ is the residual, or unexplained sample variance.

We formulate a test to reject the null hypothesis that $\mu = 0$. Consider the random variable $\widetilde{F}$ formed by taking the ratio of the explained sample variance to the unexplained sample variance. Then

$$\widetilde{F}(\omega_j) = \frac{\theta(\omega_j)}{\psi(\omega_j)}$$

$$= \frac{|\hat{\mu}(\omega_j)|^2 \sum_{k=0}^{K-1} |V_k(0;\beta,\nu)|^2}{\sum_{k=0}^{K-1} |z_k(\omega_j) - \hat{\mu}(\omega_j) V_k(0;\beta,\nu)|^2} \tag{3.26}$$

If there is a decaying sinusoid at frequency ω_j, the denominator $\psi(\omega_j)$ will be small, and thus the function $\widetilde{F}(\omega_j)$ will be large. By chance, sometimes a decaying sinusoid model will fit the time series $\{n(t)\}_{t=0}^{N-1}$ reasonably well at some frequency. The probability of this happening can be calculated. Therefore, one can describe quantitatively the confidence that there is a true signal at a given frequency.

We need to know how the random variable $\widetilde{F}(\omega_j)$ is related to the F-distribution. In Lindberg (1986) it is shown that

$$F(\omega_j) = (K-1)\widetilde{F}(\omega_j) = \frac{(K-1)\theta(\omega_j)}{\psi(\omega_j)} \tag{3.27}$$

follows an F-distribution with 2 and $(2K-2)$ degrees of freedom. Therefore, the chance that the random variable

$$F(\omega_j) = \frac{(K-1)|\hat{\mu}(\omega_j)|^2 \sum_{m=0}^{K-1} \sum_{l=0}^{K-1} \widetilde{W}_m^*(0;\beta,\nu)(\mathbf{H}^{-1})_{ml} \widetilde{W}_l(0;\beta,\nu)}{\sum_{m=0}^{K-1} \sum_{l=0}^{K-1} [y_m(\omega_j) - \hat{\mu}(\omega_j)\widetilde{W}_m(0;\beta,\nu)]^* (\mathbf{H}^{-1})_{ml} [y_l(\omega_j) - \hat{\mu}(\omega_j)\widetilde{W}_l(0;\beta,\nu)]} \tag{3.28}$$

Downloaded from https://academic.oup.com/gji/article/91/3/755/641480 by guest on 21 August 2022

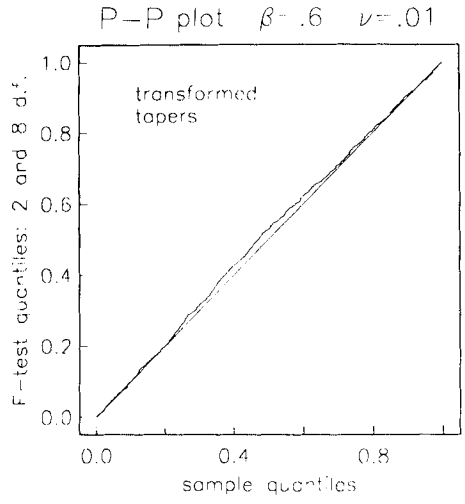

Figure 10. Ordered value, or $P-P$ plot of 675 independent values of the ratio $F(\omega_j)$ in (3.28) using synthetic stationary Gaussian white noise as input data. The cumulative probability distribution of the ordered observations $F_{(1)} \leqslant F_{(2)} \leqslant \ldots \leqslant F_{(675)}$ is plotted on the ordinant against sample quantiles on the abscissa. The jth point is plotted as the ordered pair $[(j/675), F_{(j)}]$. The graph is almost a straight line, demonstrating that the ratio $F(\omega_j)$ follows an F-distribution for Gaussian white noise input data.

takes on a particular value at some frequency due to random noise can be found using standard tables of the F-distribution (e.g. Abramowitz & Stegun 1965).

Figure 10 is an ordered value, or $P-P$ plot (Wilk & Gnanadesikan 1968) of 675 independent values of the random variable $F(\omega_j)$ generated from a synthetic record of Gaussian white noise. If the sample followed an F-distribution exactly, the ordered value plot would lie on a straight line connecting the points (0, 0) and (1, 1). The departure of the ordered value plot from a straight diagonal line is not significant at the 95 per cent confidence level, using a Kolmogorov–Smirnov test for goodness of fit (Bickel & Doksum 1977). This demonstrates graphically that the ratio $F(\omega_j)$ follows an F-distribution when the data consist of Gaussian white noise.

4 Data examples

We illustrate the multiple-taper algorithm with two examples of decaying oscillations immersed in white noise. In the first, we analyse a synthetic IDA record in which the signal-to-noise power ratio is known *a priori*. In the second, we study a 340-hr record of the 1977 Sumbawa event from IDA station NNA (Nañia, Peru). Spectral estimates made by taking the DFT of cosine-tapered data are compared to results produced by the multiple taper technique. We find the multiple-eigentaper algorithm is superior for detecting low-amplitude decaying sinusoids in noise.

We have focused our attention on the gravest observed seismic free oscillation, the spheroidal multiplet ${}_0S_2$. (${}_1S_1$ has lower frequency, but this oscillation of the inner core has not yet been conclusively observed.) The multiplet ${}_0S_2$ consists of five decaying sinusoids at distinct frequencies. These 'singlets' are labelled by an azimuthal order number $m \in \{-2, -1, 0, 1, 2\}$. The five singlet frequencies of this oscillation are widely split by the rotation of the Earth, so much so that the magnitude of the quadratic second-order Coriolis

Downloaded from https://academic.oup.com/gji/article/91/3/755/641480 by guest on 21 August 2022

splitting is roughly 60 per cent that of the quadratic splitting caused by the Earth's hydrostatic ellipticity (Dahlen & Sailor 1979). The singlet frequencies have been measured by Buland *et al.* (1979) from spherical harmonic stacks of six 150-hr IDA records of the 1977 Sumbawa event. The multiplet ${}_0S_2$ is difficult to measure as it is excited by only the very largest earthquakes. Even for the Sumbawa event, the signal-to-noise ratio is not large. Also, some singlets have very small amplitudes at some stations because of the dependence of singlet amplitude on latitude. As a result, no more than two or three of the five singlet resonance functions can be seen in any of the conventional amplitude spectra of records from the seven IDA stations existing at that time.

We constructed a 300-hr synthetic IDA record from CMO (College, Alaska) using a source located in Oaxaca, Mexico. The five singlets of ${}_0S_2$, split by rotation and ellipticity, were included in the seismogram (see Park & Gilbert (1986) for an outline of the computation procedure). Gaussian white noise was added to the record with amplitude scaled so that $N|\mu|^2/\sigma_N^2 = 73$ for the $m = 0$ singlet oscillation, $N|\mu|^2/\sigma_N^2 = 22.5$ for the $m = \pm 1$ singlets, and $N|\mu|^2/\sigma_N^2 = 3.6$ for the $m = \pm 2$ singlets. The record was sampled at 160 s intervals to produce a time series of 6750 points. We analysed the record with five eigentapers with $\Omega N = 8\pi$, $\beta = 0.6$, $\nu = 0.01$ to produce amplitude estimates $\hat{\mu}(\omega)$ and an F-test of the fit of $\hat{\mu}(\omega)$ to the complex eigenspectra. Five tapers were chosen because the five lowest order eigentapers with $\Omega N = 8\pi$, $\beta = 0.6$ and $\nu = 0.01$ have fractional leakage of 0.01 or less (Table 2). We also produced a spectral estimate using a cosine taper for comparison. According to arguments outlined in the appendix, $\langle F \rangle$ should be near the 99 per cent confidence level for the $m = \pm 1$ lines and considerably greater for the $m = 0$ line. The $m = \pm 2$ lines have $\langle F \rangle \approx 2.25$, but large random fluctuations in F are possible.

The spectral estimate using a cosine taper $|y_c(\omega)|$ is compared with the multitaper amplitude estimate $|\hat{\mu}(\omega)|$ in Fig. 11. We graph the frequency band $280 < f < 340\,\mu$Hz containing the five singlets of ${}_0S_2$ and no other known seismic free oscillation. The ordinate scales of the plots do not match because $y_c(\omega)$ is an estimated amplitude spectrum and $\hat{\mu}(\omega)$ is the amplitude of a presumed harmonic signal at $t = 0$. Many features of the plots are similar, however, because both represent discrete Fourier transforms of tapered data [$\hat{\mu}(\omega)$ corresponds to the DFT of the data times a hybrid taper as shown in (3.13)–(3.14)]. The $m = -2$, 0 and 1 singlets, having frequencies given in Table 5, are readily discernible. The prominence of the $m = -2$ singlet is puzzling in light of its low input-amplitude. The $m = -1$ singlet appears to be obscured somewhat by noise interference.

The F-test of the fit of $\hat{\mu}(\omega)$ to the complex eigenspectra is graphed in Fig. 12. All five singlets of ${}_0S_2$ are observable with better than 95 per cent detection confidence. Their measured frequencies are given in Table 5, along with estimates of the expected errors in the

Table 5. Frequencies of ${}_0S_2$ in synthetic record.

	Singlet Azimuthal Order m				
Input Singlets	−2	−1	0	1	2
Input Frequency (mHz)	.299800	.304615	.309337	.313874	.318226
Input Phase	−85°	−133°	−2.7°	126°	72°
F-Test Results					
Frequency (mHz)	.29973	.30436	.309356	.31371	.31889
Frequency Uncertainty	.00022	.00034	.000074	.00018	.00035
Phase	−74°	−118°	−1.5°	148°	87°
F-value	5.5	13.7	86.0	66.6	5.9

Downloaded from https://academic.oup.com/gji/article/91/3/755/641480 by guest on 21 August 2022

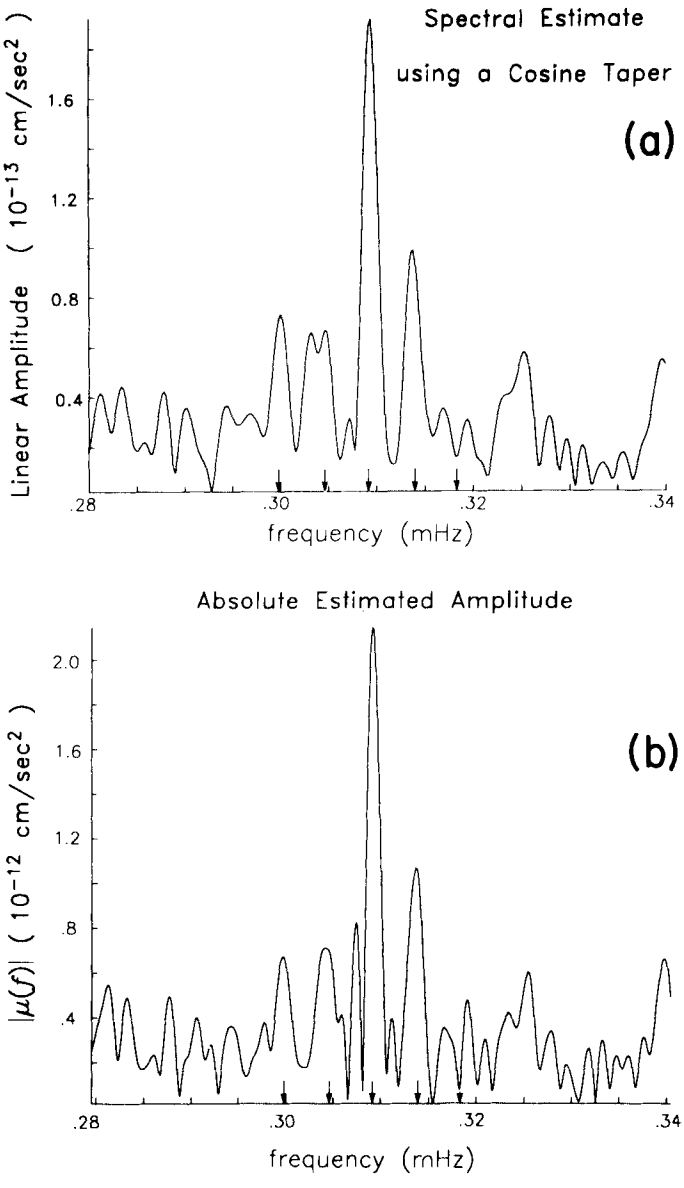

Figure 11. (a) Amplitude of a spectral estimate using a cosine taper $|y_c(\omega)|$ for a synthetic record of ${}_0S_2$. (b) The function $|\hat{\mu}(\omega)|$, where $\hat{\mu}(\omega)$ is the estimated complex amplitude of a decaying sinusoid in a synthetic record of ${}_0S_2$ using five eigentapers with parameters $\Omega N = 8\pi$, $\beta = 0.6$ and $\nu = 0.01$. In both (a) and (b), three of the five singlets of ${}_0S_2$ are visible. The true positions of the input singlets are marked.

frequencies produced by the method described in the appendix. The most poorly fit frequency observation is within 2σ of the true value. Note the rough equivalence of the F-test values for the $m = \pm 2$ singlet lines. The amplitude of the $m = -2$ singlet in Fig. 11 is enhanced by noise fluctuations, but the noise contribution has incoherent phase, causing the $m = -2$ F-test value to fall relative to that of neighbouring oscillation peaks. On the other hand, an apparent noise-minimum at the frequency of $m = +2$ single-line allows its small

Downloaded from https://academic.oup.com/gji/article/91/3/755/641480 by guest on 21 August 2022

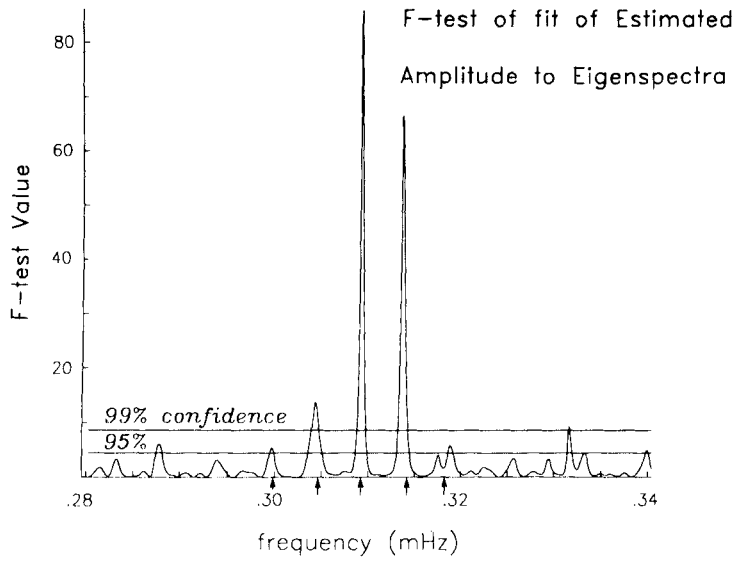

Figure 12. F-test values resulting from a test of the fit of estimated amplitude $\hat{\mu}(\omega)$ to the eigenspectra obtained using five eigentapers with parameters $\Omega N = 8\pi$, $\beta = 0.6$, and $\nu = 0.01$. The data is a synthetic record of ${}_0S_2$; it consists of five decaying sinusoids whose frequencies are listed in Table 5. All five have peaks above the 95 per cent confidence level. The function $|\hat{\mu}(\omega)|$ is plotted in Fig. 11b. The value $F = 3.11$ corresponds to the 90 per cent confidence level, $F = 4.46$ is the 95 per cent confidence level, and $F = 8.65$ is the 99 per cent level. The true positions of the input singlets are marked.

amplitude to be detectable in the plot of the F-test. Note also that the F-test has peaks at frequency values not associated with ${}_0S_2$ singlets. These are caused by random statistical fluctuations. The frequency band shown contains 65 independent frequency samples. Therefore, one would expect that due to randomness, roughly three values of the F-test in Fig. 12 would protrude above $F \approx 4.5$, the 95 per cent confidence level for the F-distribution.

We also took 340 hr of vertical IDA gravimeter data from station NNA, starting 8.5 hr after the onset of the Sumbawa event. This record is relatively complete, with only two data gaps of roughly 2.5 hr each at 95 and 275 hr into the record. Time series points falling in the gaps were assigned the value zero. The data were sampled at 20 s intervals. We low-pass filtered and decimated the record so that it contained 7668 points taken at 160 s intervals. Aftershocks that did not visibly affect the instrument in a non-linear manner were retained, as their effect on the spectrum in the vicinity of ${}_0S_2$ is small. Sections exhibiting non-linear seismometer response contribute significant energy at low frequencies, and so these were removed.

We had to know roughly the Q's of the singlets of ${}_0S_2$ to apply our procedure. The $Q \simeq 560$ value for ${}_0S_2$ given by the model of Masters & Gilbert (1983) corresponds to $\beta = 0.68$. Chao & Gilbert (1980) estimate that the $m = 2$ singlet of ${}_0S_2$ has a Q of 415, the $m = 0$ singlet has a Q of 609 and the $m = 2$ singlet has a Q of 509. The Q measurement reported by Hansen & Schnapp (1982) leads to a decay parameter of $\beta = 0.84$. We analysed the record with a set of five eigentapers having parameters $\Omega N = 8\pi$, $\nu = 0.01$ and $\beta = 0.65$.

The function $|\hat{\mu}(\omega)|$ obtained using the eigentapers is plotted in Fig. 13b, and the amplitude of the spectral estimate using the cosine taper $|y_c(\omega)|$ is presented in Fig. 13a. Again, we graph the frequency band $280 < f < 340\,\mu$Hz. Spectra were calculated at frequencies separated by $0.163\,\mu$Hz using the DFT. Table 6 lists the frequency estimates of the five

Downloaded from https://academic.oup.com/gji/article/91/3/755/641480 by guest on 21 August 2022

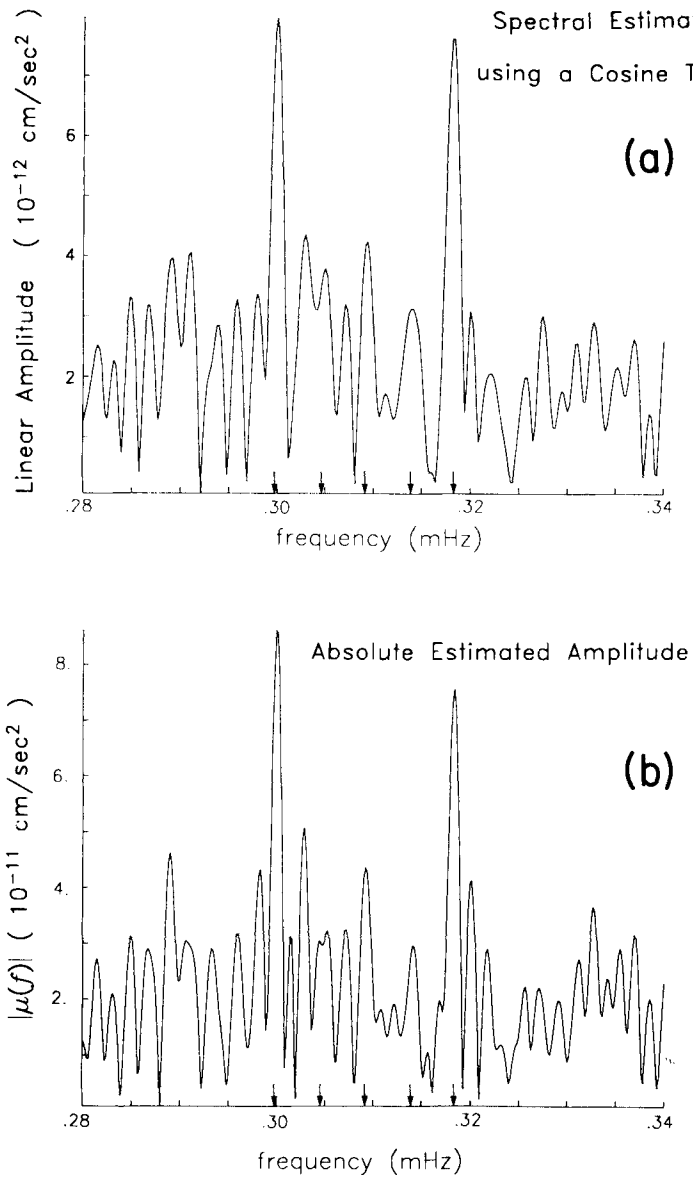

Figure 13. (a) Amplitude of a spectral estimate using a cosine taper for a time series of the Sumbawa event recorded at IDA station NNA. We plot the frequency band $280 < f < 340\,\mu$Hz containing the five ${}_0S_2$ singlets. Only two of the singlets are observable. (b) Amplitude of the function $\hat{\mu}(\omega)$ for a time series of the Sumbawa event recorded at IDA station NNA. We plot the frequency band $280 < f < 340\,\mu$Hz containing the five ${}_0S_2$ singlets, but again only two singlets are visible. The positions of the five singlets as determined by stacking are indicated.

singlets of ${}_0S_2$ made by Buland *et al.* (1979); these frequencies are marked in Fig. 13a and b. Only the $m = \pm 2$ lines are clearly visible in Fig. 13a and b. Candidates for the other singlet resonances are evident but do not protrude significantly above the apparent ambient noise level.

Figure 14 is a graph of the F-test of the fit of $\hat{\mu}(\omega)$ to the complex eigenspectra. There are

Downloaded from https://academic.oup.com/gji/article/91/3/755/641480 by guest on 21 August 2022

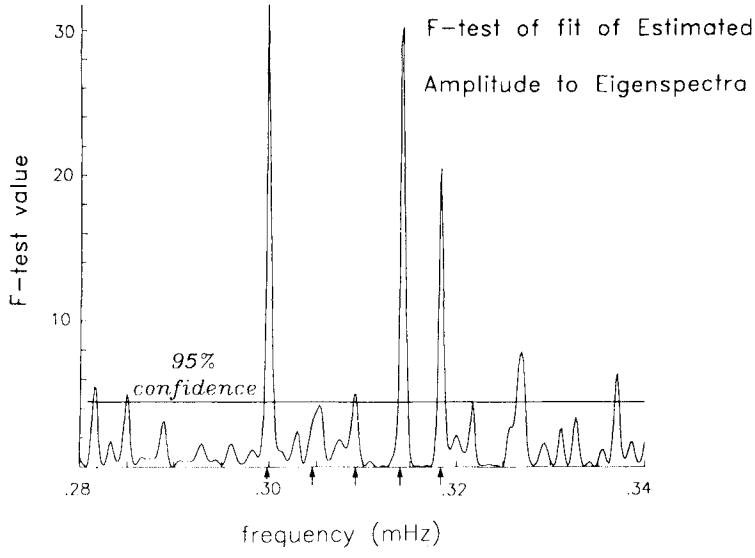

Figure 14. F-test for the estimated amplitude $\hat{\mu}(\omega)$ plotted in Fig. 13a. The time series being analysed is a record of Sumbawa event from IDA station NNA. We plot the frequency band $280 < f < 340\,\mu$Hz containing the five ${}_0S_2$ singlets. Four of the singlets have F-test peaks corresponding to greater than 95 per cent confidence of detection. The positions of the five singlets as determined by stacking are indicated.

four peaks above the 95 per cent detection confidence level in Fig. 14 which correspond to singlets of ${}_0S_2$. The $m = -1$ singlet appears to be contaminated by noise, resulting in a low, asymmetric variance-ratio peak. The estimated frequencies of all five lines, and their associated uncertainties, are listed in Table 6. The discrepancy between the $m = -1$ frequency estimate and that of Buland *et al.* (1979) is another indicator of the noise contamination of the $m = -1$ singlet. The other peaks in Fig. 14 above the 95 per cent confidence level are most likely due to random fluctuations.

In the above examples, we knew (approximately) the frequencies of the decaying oscillations and that they had large enough amplitude to be detectable. To be useful, the multitaper detection algorithm for decaying sinusoids should yield comparable results when either or both of the above conditions are not satisfied. Given the known frequencies of the gravest seismic oscillations, one could use the algorithm to search for so-called 'silent' events (e.g. Kanamori & Cipar 1974), whose existence is still controversial. In the more conservative enterprise of expanding and refining the free-oscillation data set in order to constrain deep Earth structure more reliably, the eigentaper algorithm offers hope of retrieving more

Table 6. Frequencies of ${}_0S_2$ in NNA record of Sumbawa event.

	Singlet Azimuthal Order m				
F-Test Results	−2	−1	0	1	2
Frequency (mHz)	.29988	.30526	.30918	.31423	.31830
Frequency Uncertainty	.00027	.00060	.00041	.00016	.00013
Phase	−134°	−48°	−43°	142°	10°
F-Value	31.7	4.2	5.0	30.0	20.5
From Buland *et al.* (1979)					
Frequency (mHz)	.300010	.304799	.309490	.314000	.318499

Downloaded from https://academic.oup.com/gji/article/91/3/755/641480 by guest on 21 August 2022

marginally observable modes than are accessible using single-taper algorithms. Care must be exercised that peaks in the F-test due to random noise are not misidentified as seismic free-oscillations. To this end, quantitative comparison of more than one seismic record is essential. This has been done by combining the standard techniques of stacking and stripping of low-frequency seismic records (Gilbert & Dziewonski 1975) with the multitaper algorithm. This is discussed in Part II of this paper.

5 Summary

We have described a variational procedure for determining tapers that optimally resist spectral leakage from outside a frequency region of bandwidth 2Ω for exponentially decaying sinusoids contaminated by white noise. Multiplying the data by these tapers creates a number of time series. A decaying sinusoid model is fitted to the discrete Fourier transforms of the tapered data series at each frequency of interest (equation 3.15). The fit of this model to the data is tested at each frequency using a statistical F-test (equation 3.28). This gives a quantitative measure of the chance that there is a decaying sinusoid at any given frequency in the data. We have shown that this procedure is a sensitive detector of decaying harmonic lines in free oscillation data.

In Part II of this paper, we shall present a number of extensions to the multiple-taper method of harmonic analysis. We shall explain how the technique has been modified to estimate the harmonic components of records containing gaps. We discuss how sinusoids at frequencies between the discrete FFT bin frequencies can be detected, and how this method can be combined with conventional multi-station stacking procedures. The resolution of closely spaced harmonic lines is treated. Subsequently, we plan to introduce algorithms for finding the decay rates of free oscillations, as well as their frequencies.

Acknowledgments

The authors would like to thank Drs Freeman Gilbert, Robert L. Parker and Alan D. Chave for their encouragement during this work. Dr John Rice helped us with some of the statistical definitions. Guy Masters provided us with edited IDA records for exploratory data analysis. This work was supported by National Science Fundation Grant EAR-84-09612 and Office of Naval Research contracts N00014-85-C-0104 and N00014-80-C-0440; D. J. Thomson was partially supported by the La Jolla Foundation for Earth Sciences during his stay at the Institute of Geophysics and Planetary Physics as a Green Scholar during 1983.

References

Abramowitz, M. & Stegun, I. A. (eds), 1965. *Handbook of Mathematical Functions,* Dover, New York.

Agnew, D. C. & Berger, J., 1978. Vertical seismic noise at very low frequencies, *J. geophys. Res.*, **83,** 5420–5424.

Agnew, D. C., Berger, J., Buland, R., Farrell, W. & Gilbert, F., 1976. International deployment of accelerometers: A network for very long period seismology, *Eos, Trans. Am. geophys. Un.*, **57,** 180–188.

Bickel, P. J. & Doksum, K. A., 1977. *Mathematical Statistics: Basic Ideas and Selected Topics,* Holden-Day, San Francisco.

Brigham, E. O., 1974. *The Fast Fourier Transform,* Prentice-Hall, Englewood Cliffs, NJ.

Buland, R. & Gilbert, F., 1978. Improved resolution of complex eigenfrequencies in analytically continued seismic spectra, *Geophys. J. R. astr. Soc.*, **52,** 457–470.

Buland, R., Berger, J. & Gilbert, F., 1979. Observations from the IDA network of attenuation and splitting during a recent earthquake, *Nature,* **277,** 358–362.

Downloaded from https://academic.oup.com/gji/article/91/3/755/641480 by guest on 21 August 2022

Chao, B. F. & Gilbert, F., 1980. Autoregressive estimation of complex eigenfrequencies in low-frequency seismic spectra, *Geophys. J. R. astr. Soc.*, **63**, 641–657.

Cooley, J. W. & Tukey, J., 1965. An algorithm for the machine calculation of complex Fourier series, *Maths Comput.*, **19**, 297–301.

Dahlen, F. A., 1982. The effect of data windows on the estimation of free oscillation parameters, *Geophys. J. R. astr. Soc.*, **69**, 537–549.

Dahlen, F. A. & Sailor, R., 1979. Rotational and elliptical splitting of the free oscillations of the Earth, *Geophys. J. R. astr. Soc.*, **58**, 609–623.

Engdahl, E. R., Peterson, J. & Orsini, N. A., 1982. Global digital networks – Current status and future directions, *Bull. seism. Soc. Am.*, **72**, S243–S259.

Gilbert, F. & Backus, G., 1965. The rotational splitting of the free oscillations of the Earth; 2, *Rev. Geophys. Space Phys.*, **3**, 1–9.

Gilbert, F. & Dziewonski, A. M., 1975. An application of normal mode theory to the retrieval of structural parameters and source mechanisms from seismic spectra, *Phil. Trans. R. Soc. A*, **278**, 187–269.

Goldstein, H., 1980. *Classical Mechanics*, 2nd edn, Addison-Wesley, Menlo Park, CA.

Golub, G. H. & VanLoan, C. F., 1983. *Matrix Computations*, Johns Hopkins University Press, Baltimore.

Hansen, R. A. & Schnapp, M. G., 1982. Estimation of the Q of split mode free oscillations (abstract), *Eos, Trans. Am. geophys. Un.*, **63**, 1034.

Harris, F. J., 1978. On the use of windows for harmonic analysis with the discrete Fourier transform, *Proc. IEEE*, **66**, 51–83.

Jones, R. H., 1962. Spectral estimates and their distributions, in *Skandinavisk Actuatietidskrift*, **45**, Part I: 39–69, Part II: 135–153.

Kanamori, H. & Cipar, J. J., 1974. Focal process of the great Chilean Earthquake May 22, 1960, *Phys. Earth planet. Int.*, **9**, 128–136.

Kendall, M. & Stuart, A., 1979. *The Advanced Theory of Statistics*, vol. 2, 4th edn, Macmillan, New York.

Landau, H. J. & Pollak, H. O., 1961. Prolate spheroidal wave functions, Fourier analysis and uncertainty – II, *Bell Systems Tech. J.*, **40**, 65–84.

Landau, H. J. & Pollak, H. O., 1962. Prolate spheroidal wave functions, Fourier analysis and uncertainty – III, *Bell Systems Tech. J.*, **40**, 1295–1336.

Lindberg, C., 1986. Multiple taper harmonic analysis of terrestrial free oscillations, *PhD Thesis*, University of California.

Lindberg, C. R., Vernon III, F. L. & Park, J. J., 1988. Comparison of conventional and multitaper spectral estimation methods on synthetic high frequency seismic wavetrains.

Luenberger, D. G., 1969. *Optimization by Vector Space Methods*, John Wiley and Sons, New York.

Masters, T. G. & Gilbert, F., 1981. Structure of the inner core inferred from observations of its spheroidal shear modes, *Geophys. Res. Lett.*, **8**, 569–571.

Masters, G. & Gilbert, F., 1983. Attenuation in the earth at low frequencies, *Phil. Trans. R. Soc. A*, **308**, 479–522.

Miller, K. S., 1974. *Complex Stochastic Processes: An Introduction to Theory and Application*, Addison-Wesley, Reading, MA.

Park, J. & Gilbert, F., 1986. Coupled free oscillations of an aspherical, dissipative, rotating Earth: Galerkin theory, *J. geophys. Res.*, **91**, 7241–7260.

Park, J., Lindberg, C. R. & Vernon III, F. L., 1987. Multitaper spectral analysis of high frequency seismograms, *J. geophys. Res.*, in press.

Riedesel, M. A., Agnew, D. C., Berger, J. & Gilbert, F., 1980. Stacking for the frequencies and Q's of ${}_0S_0$ and ${}_1S_0$, *Geophys. J. R. astr. Soc.*, **62**, 457–471.

Slepian, D., 1964. Prolate spheroidal wave functions, Fourier analysis and uncertainty – IV, *Bell Systems Tech. J.*, **43**, 3009–3057.

Slepian, D., 1978. Prolate spheroidal wave functions, Fourier analysis and uncertainty – V: The discrete case, *Bell Systems Tech. J.*, **57**, 1371–1429.

Slepian, D., 1983. Some comments on Fourier analysis, uncertainty and modeling, *SIAM Rev.*, **25**, 379–393.

Slepian, D. & Pollak, H. O., 1961. Prolate spheroidal wave functions, Fourier analysis and uncertainty – I, *Bell Systems Tech. J.*, **40**, 43–64.

Smith, B. T., Boyle, J. M., Dongerra, J. J., Garbow, B. S., Ikebe, Y., Klema, V. C. & Moler, C. B., 1976. Matrix Eigensystem Routines – EISPACK Guide, Lecture Notes in *Computer Science*, Springer-Verlag, New York.

Smith, D. R., 1974. *Variational Methods in Optimization*, Prentice-Hall, Englewood Cliffs, NJ.

Downloaded from https://academic.oup.com/gji/article/91/3/755/641480 by guest on 21 August 2022

Thomson, D. J., 1982. Spectrum estimation and harmonic analysis, *Proc. IEEE*, **70**, 1055–1096.
Tukey, J. W., 1975. Instead of Gauss-Markov least squares, what? in *Applied Statistics*, pp. 351–372, ed. Gupta, R. P., North-Holland Publishing House, Amsterdam.
Wilk, M. B. & Gnanadesikan, R., 1968. Probability plotting methods for the analysis of data, *Biometrica*, **55**, 1–17.
Wonnacott, T. H. & Wonnacott, R. J., 1981. *Regression: A Second Course in Statistics*, John Wiley, New York.

Appendix: error estimation

The methods of Section 3 can be used to obtain estimates of the complex amplitude and the frequency of a decaying sinusoid in a time series. Random noise can cause the estimated amplitude and estimated frequency to deviate from the true values. This appendix outlines methods for calculating the expected size of these deviations.

A1 Estimated amplitude

First, consider the estimated amplitude $\hat{\mu}(\hat{\omega})$. It is a statistical estimator of the true amplitude μ. The utility of $\hat{\mu}$ as an estimator can be gauged by its bias $\langle\hat{\mu}\rangle - \mu$ and its mean square error $\langle|\hat{\mu} - \mu|^2\rangle$. Let the data $x(t)$ be zero mean white noise $n(t)$ plus a decaying sinusoid with frequency ω_T. Then

$$x(t) = n(t) + \mu \exp(i\omega_T t - \alpha t); \qquad t = 0, 1, \ldots, N-1 \tag{A.1}$$

where μ is the true complex amplitude, α is the true decay rate, and $\langle n(t) n^*(t')\rangle = \sigma_N^2 \delta_{tt'}$. We also assume that $\langle n(t) n(t')\rangle = 0$. [This is justified as only the real part of the $n(t)$ is actually measured, leaving us free to define its imaginary part. Miller (1974, p. 41) gives further details.] The kth transformed complex eigenspectrum of the data is

$$\begin{aligned} z_k(\omega) &= (\mathbf{G}^{-1})_{kl} y_l(\omega) \\ &= g_k(\omega) + \mu V_k(\omega - \omega_T; \beta, \nu), \end{aligned} \tag{A.2}$$

where

$$g_k(\omega) = (\mathbf{G}^{-1})_{kl} \sum_{t=0}^{N-1} \exp(-i\omega t)\, w_l(t; \beta, \nu)\, n(t)$$

and $\mathbf{G}$, $y_l(\omega)$ and V_k are as defined in Section 3. It follows that

$$\langle z_k(\omega)\rangle = \mu V_k(\omega - \omega_T; \beta, \nu) \tag{A.3}$$

and

$$\langle z_k(\omega) z_l^*(\omega)\rangle = \sigma_N^2 \delta_{kl} + |\mu|^2 V_k(\omega - \omega_T; \beta, \nu)\, V_l^*(\omega - \omega_T; \beta, \nu). \tag{A.5}$$

The expected value of $\hat{\mu}$, combining (3.13) and (A.3) is

$$\langle\hat{\mu}(\omega)\rangle = \frac{\mu \sum_{k=0}^{K-1} V_k^*(0; \beta, \nu)\, V_k(\omega - \omega_T; \beta, \nu)}{\sum_{k=0}^{K-1} |V_k(0; \beta, \nu)|^2}. \tag{A.6}$$

Downloaded from https://academic.oup.com/gji/article/91/3/755/641480 by guest on 21 August 2022

When $\omega = \omega_T$, $\langle \hat{\mu}(\omega_T) \rangle = \mu$, so $\hat{\mu}$ is unbiased at the true frequency ω_T. At other frequencies $\hat{\mu}$ is a biased estimator of μ.

The mean square error of $\hat{\mu}$ is constant at all frequencies, and using (A.6), is

$$\langle | \hat{\mu} - \mu |^2 \rangle = \frac{\sigma_N^2}{\rho}, \tag{A.7}$$

where

$$\rho = \sum_{k=0}^{K-1} | V_k(0; \beta, \nu) |^2$$

A2 Frequency estimates

Now consider the estimation of the true frequency ω_T. The true frequency can be estimated from (1) the frequencies of peaks in the modulus of the estimated amplitude $|\hat{\mu}|^2$, (2) minima in the unexplained sample variance $\psi(\omega_j)$ introduced in (3.25), or (3) peaks in the random variable $F(\omega_j) = (K-1)\theta(\omega_j)/\psi(\psi_j)$. These all provide approximately unbiased estimates of the true frequency ω_T, and their mean square errors can be computed, as shown below.

A2.1 FREQUENCIES ESTIMATED FROM PEAKS IN $|\hat{\mu}|^2$

The function $|\hat{\mu}(\omega)|^2$ achieves a peak at frequency ω_θ, where

$$0 = \theta'(\omega_\theta) = \left(\frac{d}{d\omega} |\hat{\mu}(\omega)|^2 \Big|_{\omega = \omega_\theta} \right) \rho. \tag{A.8}$$

In a neighbourhood of the true frequency ω_T

$$0 = \theta'(\omega_\theta) \approx \theta'(\omega_T) + (\omega_\theta - \omega_T)\theta''(\omega_T). \tag{A.9}$$

Taking expectation values of both sides, and assuming that $(\omega_\theta - \omega_T)$ and $\theta''(\omega_T)$ are uncorrelated:

$$\langle \omega_\theta - \omega_T \rangle \approx \frac{-\langle \theta'(\omega_T) \rangle}{\langle \theta''(\omega_T) \rangle}. \tag{A.10}$$

Define the matrix $\mathbf{M}^{(j)}$ with elements

$$M_{ml}^{(j)} = (m - l)^j; \qquad m, l = 0, 1, 2, \ldots, N-1, \tag{A.11}$$

where j is an integer, and the vector $\hat{\mathbf{v}}$ with elements

$$\hat{v}(t) = \frac{\sum_{k=0}^{K-1} V_k^*(0; \beta, \nu) v_k(t; \beta, \nu)}{\rho} \exp(-\alpha t); \qquad t = 0, 1, 2, \ldots, N-1. \tag{A.12}$$

Then some algebra shows that

$$\langle \theta'(\omega_T) \rangle = -i |\mu|^2 \rho \hat{\mathbf{v}} \cdot \mathbf{M}^{(1)} \cdot \hat{\mathbf{v}} = 0 \tag{A.13}$$

as $\mathbf{M}^{(1)}$ is antisymmetric, and

$$\langle \theta''(\omega_T) \rangle = -\rho |\mu|^2 \hat{\mathbf{v}} \cdot \mathbf{M}^{(2)} \cdot \hat{\mathbf{v}}. \tag{A.14}$$

Downloaded from https://academic.oup.com/gji/article/91/3/755/641480 by guest on 21 August 2022

Therefore, from (A.10), $\langle \omega_\theta - \omega_T \rangle = 0$ and ω_θ is an unbiased estimator of ω_T. To find the mean square error of ω_θ, square both sides of (A.9) and take expected values:

$$\langle (\omega_\theta - \omega_T)^2 \rangle \approx \frac{\langle [\theta'(\omega_T)]^2 \rangle}{\langle [\theta''(\omega_T)]^2 \rangle}. \tag{A.15}$$

Using the relation

$$\begin{aligned}\langle x(t_1)x^*(t_2)x(t_3)x^*(t_4)\rangle = {} & |\mu|^4 \exp[i\omega_T(t_1 - t_2 + t_3 - t_4)] \exp[-\alpha(t_1 + t_2 + t_3 + t_4)] \\ & + \sigma_N^2 |\mu|^2 \delta_{t_1 t_2} \exp[i\omega_T(t_3 - t_4) - \alpha(t_3 + t_4)] \\ & + \delta_{t_3 t_4} \exp[i\omega_T(t_1 - t_2) - \alpha(t_1 + t_2)] \\ & + \delta_{t_1 t_4} \exp[i\omega_T(t_3 - t_2) - \alpha(t_3 + t_2)] \\ & + \delta_{t_2 t_3} \exp[i\omega_T(t_1 - t_4) - \alpha(t_1 + t_4)] \\ & + \sigma_N^4 (1 + \tfrac{1}{2}\delta_{t_1 t_3})(\delta_{t_1 t_2}\delta_{t_3 t_4} + \delta_{t_1 t_4}\delta_{t_2 t_3})\end{aligned} \tag{A.16}$$

one finds that

$$\langle [\theta'(\omega_T)]^2 \rangle = \rho \{\sigma_N^4 \, \mathbf{s} \cdot \mathbf{M}^{(2)} \cdot \mathbf{s} + 2\sigma_N^2 |\mu|^2 \mathbf{s} \cdot \mathbf{r}\} \tag{A.17}$$

and

$$\langle [\theta''(\omega_T)]^2 \rangle = \rho \{\sigma_N^4 \, \mathbf{s} \cdot \mathbf{M}^{(4)} \cdot \mathbf{s} + 2\sigma_N^2 |\mu|^2 \mathbf{s} \cdot \mathbf{r} + |\mu|^4 (\mathbf{v} \cdot \mathbf{M}^{(2)} \cdot \hat{\mathbf{v}})^2\}, \tag{A.18}$$

where $\mathbf{s}$ has components

$$s_t = [\hat{v}(t) \exp(\alpha t)]^2; \qquad t = 0, 1, \ldots, N-1 \tag{A.19}$$

and $\mathbf{r}$ has components

$$r_t = [(\mathbf{M}^{(2)} \cdot \hat{\mathbf{v}})_t]^2; \qquad t = 0, 1, \ldots, N-1. \tag{A.20}$$

For sufficiently large initial signal-to-noise ratios, $N|\mu|^2/\sigma_N^2 \gg 1$, and

$$\langle (\omega_\theta - \omega_T)^2 \rangle \approx \frac{2\sigma_N^2}{|\mu|^2} \frac{\mathbf{s} \cdot \mathbf{r}}{\hat{\mathbf{v}} \cdot \mathbf{M}^{(2)} \cdot \hat{\mathbf{v}}}. \tag{A.21}$$

The mean-square error of the estimator ω_θ decreases as the signal-to-noise ratio increases.

Figure A1 is a plot of the estimated rms misfit of ω_θ, defined by

$$\langle \omega_\theta - \omega_T \rangle_{\text{rms}} \equiv \sqrt{\langle (\omega_\theta - \omega_T)^2 \rangle}$$

as a function of initial signal-to-noise ratio for tapers with parameters $\beta = 0.6$, 1.05 and $\nu = 0$, 0.01, 0.1, 1 using (A.15). The misfit is plotted on the ordinate as a fraction of the Rayleigh frequency $\omega_R = 2\pi/T$, where $T = N\Delta t$. The parameter $N|\mu|^2/\sigma_N^2$ is plotted on the abscissa. One expects frequency uncertainty to increase rapidly with decreasing signal-to-noise ratio, but for $N|\mu|^2/\sigma_N^2 < 10$, the estimated frequency uncertainty in Fig. A1 is essentially constant. This is because relation (A.15) ceases to be a good approximation at low signal-to-noise ratios, where the first-order expansion (A.9) fails to hold, and $(\omega_\theta - \omega_T)$ and $\theta''(\omega_T)$ are correlated. The solid curve corresponds to $\nu = 0$; larger values of ν correspond to succeedingly finer dashed curves. The rms misfit $\langle \omega_\theta - \omega_T \rangle_{\text{rms}}$ tends to decrease with decreasing values of ν (except for $\beta = 1.05$ and $N|\mu|^2/\sigma_N^2 > 80$).

Downloaded from https://academic.oup.com/gji/article/91/3/755/641480 by guest on 21 August 2022

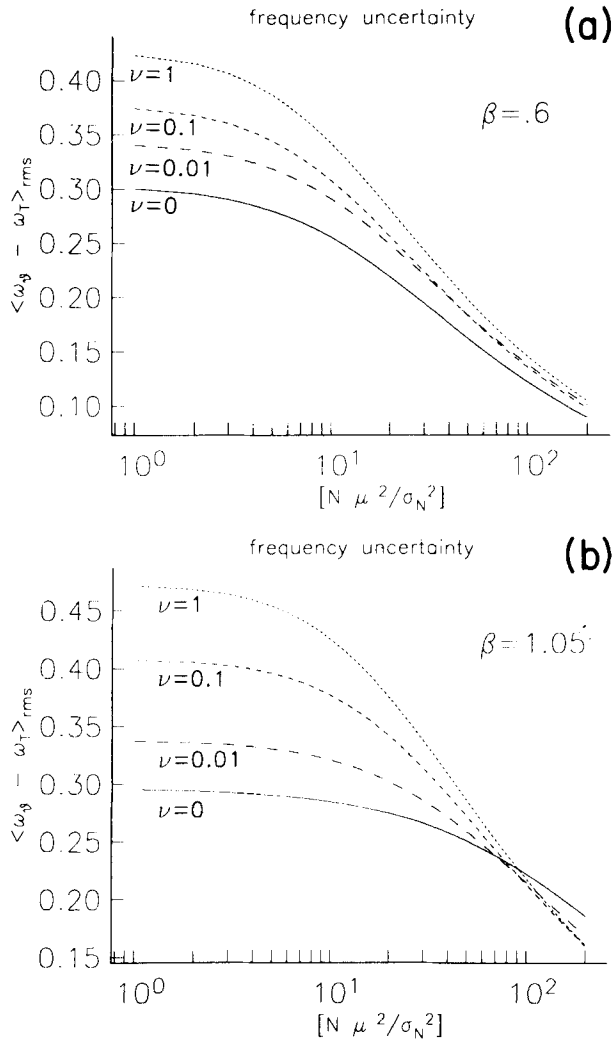

Figure A1 (a, b). Estimated rms misfit of estimated frequency ω_θ to true frequency ω_T as a function of $N|\mu|^2/\sigma_N^2$ for tapers with $\Omega N = 8\pi$, $\beta = 0.6$, 1.05 and $\nu = 0$, 0.01, 0.1 and 1. The curves are meaningless for $N|\mu|^2/\sigma_N^2 < 10$ because (A.15) fails to be a good approximation. Uncertainty decreases with decreasing values of noise parameter ν (except for $\beta = 1.05$ and $N|\mu|^2/\sigma_N^2 > 80$). Uncertainty decreases with increasing signal-to-noise ratio.

A2.2 FREQUENCIES ESTIMATED FROM MINIMA IN $\psi(\omega)$

Another estimator of the true frequency ω_T is ω_ψ, the frequency of a minimum in the unexplained sample variance defined by

$$\psi'(\omega_\psi) = 0$$

The frequency ω_ψ is also an unbiased estimator of ω_T, as

$$\langle \omega_\psi - \omega_T \rangle \approx -\frac{\langle \psi'(\omega_T) \rangle}{\langle \psi''(\omega_T) \rangle} = 0. \tag{A.22}$$

Downloaded from https://academic.oup.com/gji/article/91/3/755/641480 by guest on 21 August 2022

The result (A.22) can be obtained using (3.25) and (A.13):

$$\langle \psi'(\omega_T) \rangle = \langle \xi'(\omega_T) \rangle = \sum_{k=0}^{K-1} \left\langle \left(\frac{d}{d\omega} |z_k(\omega)|^2 \right)_{\omega=\omega_T} \right\rangle$$

$$= -i|\mu|^2 \sum_{k=0}^{K-1} \sum_{t=0}^{N-1} \sum_{t'=0}^{N-1} (t-t') v_k(t) v_k(t') \exp[-\alpha(t+t')] = 0. \tag{A.23}$$

Also,

$$\langle \psi''(\omega_T) \rangle = -|\mu|^2 tr(\mathbf{M}^{(2)} \cdot \mathbf{\Gamma}^{(1)}) > 0, \tag{A.24}$$

where the matrix $\mathbf{\Gamma}^{(j)}$ has components

$$\Gamma_{tt'}^{(j)} = \sum_{k=0}^{K-1} [v_k(t) v_k(t') - |V_k(0;\beta,\nu)|^2 s_t s_{t'}]^j; \qquad t, t' = 0, 1, \ldots, N-1 \tag{A.25}$$

and *tr* denotes the trace operation on matrices. Define also the matrix $\Gamma^{[\mu,\nu]}$ with components

$$\Gamma_{tt'}^{[\mu,\nu]} = \Gamma_{tt'}^{(1)} \exp(-\mu t) \exp(-\nu t'); \qquad t, t' = 0, 1, \ldots, N-1. \tag{A.26}$$

Then the mean square error of estimator ω_ψ can be approximated as

$$\langle (\omega_\psi - \omega_T)^2 \rangle \approx \frac{\langle [\psi'(\omega_T)]^2 \rangle}{\langle [\psi''(\omega_T)]^2 \rangle}, \tag{A.27}$$

where

$$\langle [\psi'(\omega_T)]^2 \rangle = \sigma_N^4 \operatorname{tr}(\mathbf{M}^{(2)} \cdot \mathbf{\Gamma}^{(2)}) + 2\sigma_N^2 |\mu|^2 \sum_{t=0}^{N-1} [(\mathbf{M}^{(1)} \cdot \mathbf{\Gamma}^{[0,\alpha]})_{tt}]^2 \tag{A.28}$$

and

$$\langle [\psi''(\omega_T)]^2 \rangle = \sigma_N^4 \operatorname{tr}(\mathbf{M}^{(4)} \cdot \mathbf{\Gamma}^{(2)}) + 2\sigma_N^2 |\mu|^2 \sum_{t=0}^{N-1} [(\mathbf{M}^{(2)} \cdot \mathbf{\Gamma}^{[0,\alpha]})_{tt}]^2 + |\mu|^4 [\operatorname{tr}(\mathbf{M}^{(2)} \cdot \mathbf{\Gamma}^{[\alpha,\alpha]})]^2. \tag{A.29}$$

For $N|\mu|^2/\sigma_N^2 \gg 1$:

$$\langle (\omega_\psi - \omega_T)^2 \rangle \approx \left(\frac{\sigma_N^2}{|\mu|^2} \right) \cdot \frac{2 \sum_{t=0}^{N-1} [(\mathbf{M}^{(1)} \cdot \mathbf{\Gamma}^{[0,\alpha]})_{tt}]^2}{[\operatorname{tr}(\mathbf{M}^{(2)} \mathbf{\Gamma}^{[\alpha,\alpha]})]^2}. \tag{A.30}$$

As signal-to-noise ratio increases, $\langle (\omega_\psi - \omega_T)^2 \rangle$ becomes smaller. Graphs of $\langle \omega_\psi - \omega_T \rangle_{rms} = \sqrt{\langle (\omega_\psi - \omega_T)^2 \rangle}$ have the same shape as the plots of $\langle \omega_\theta - \omega_T \rangle_{rms}$ in Fig. A1, but $\langle \omega_\psi - \omega_T \rangle_{rms}$ is 10–25 per cent larger than $\langle \omega_\theta - \omega_T \rangle_{rms}$ for a given signal-to-noise ratio. For example, if $\beta = \nu = 0$ and $N|\mu|^2/\sigma_N^2 = 10$, $\langle \omega_\theta - \omega_T \rangle_{rms} = 0.136\,\omega_R$, and $\langle \omega_\psi - \omega_T \rangle_{rms} = 0.165\,\omega_R$.

A2.3 FREQUENCIES ESTIMATED FROM PEAKS IN $F(\omega)$

The true frequency ω_T can also be estimated from the frequencies ω_F of peaks in the F-test curve defined by $F'(\omega_F) = 0$. As before, to first-order in $(\omega_F - \omega_T)$, assuming $(\omega_F - \omega_T)$

Downloaded from https://academic.oup.com/gji/article/91/3/755/641480 by guest on 21 August 2022

and $F''(\omega_T)$ are uncorrelated:

$$\langle \omega_F - \omega_T \rangle \approx - \frac{\langle F''(\omega_T) \rangle}{\langle F''(\omega_T) \rangle}. \tag{A.31}$$

By (3.27),

$$\psi^2(\omega) F'(\omega) = (K-1)\,[\theta'(\omega)\,\psi(\omega) - \theta(\omega)\,\psi'(\omega)]. \tag{A.32}$$

Assume that ψ^2 and F', θ' and ψ, and θ and ψ' are uncorrelated at ω_T. Then, the expectation value of the right hand side of (A.32) vanishes at $\omega = \omega_T$. But,

$$\langle \psi^2(\omega_T) \rangle = \sigma_N^4 \left(\sum_{t=0}^{N-1} [v_k(t; \beta, \nu)]^2 \right)^2 \neq 0$$

so $\langle F'(\omega_T) \rangle = 0$. As $\langle F''(\omega_T) \rangle < 0$, ω_F is an unbiased estimator of ω_T by (A.31).

The frequency ω_F can be expressed in terms of ω_θ and ω_ψ. Expanding $\theta(\omega_F)$ and $\psi(\omega_F)$ in power series about their extrema to second-order in $(\omega_F - \omega_\theta)$ and $(\omega_F - \omega_\psi)$:

$$F(\omega_F) \approx \frac{(K-1)\,[\theta(\omega_\theta) + \tfrac{1}{2}(\omega_F - \omega_\theta)^2 \theta''(\omega_\theta)]}{\psi(\omega_\psi) + \tfrac{1}{2}(\omega_F - \omega_\psi)^2 \psi''(\omega_\psi)} \tag{A.33}$$

and

$$(\omega_F - \omega_\theta) \frac{\theta''(\omega_\theta)}{\psi''(\omega_\psi)} \approx \frac{(\omega_F - \omega_\psi) F(\omega_F)}{K-1} \tag{A.34}$$

from (A.33). Substitute (A.33) in (A.34) and let

$$\omega_F = \tilde{\omega} \frac{(\omega_\psi - \omega_\theta)}{2} + \frac{(\omega_\psi + \omega_\theta)}{2} \tag{A.35}$$

so that $\omega_F = \omega_\psi$ when $\tilde{\omega} = 1$, and $\omega_F = \omega_\theta$ when $\tilde{\omega} = -1$. Then $\tilde{\omega}$ satisfies

$$\tilde{\omega}^2 - 2(a+b)\,\tilde{\omega} - (1 + 2b - 2a) = 0, \tag{A.36}$$

where

$$a = \frac{-2\theta(\omega_\theta)}{(\omega_\psi - \omega_\theta)^2 \theta''(\omega_\theta)}$$

$$b = \frac{2\psi(\omega_\psi)}{(\omega_\psi - \omega_\theta)^2 \psi''(\omega_\psi)}.$$

The two solutions of the quadratic equation (A.36) are

$$\tilde{\omega}_\pm = (a+b) \pm \sqrt{(a+b)^2 + 2b + 1 - 2a}. \tag{A.37}$$

The solution $\tilde{\omega}_+$ is spurious because $|\tilde{\omega}_+| \to \infty$ as a or $b \to \infty$, and truncated Taylor series expansions in (A.33) and (A.34) are invalid for large values of $\tilde{\omega}$. The second solution $\tilde{\omega}_-$ is constrained so that $|\tilde{\omega}_-| < 1$, and corresponds to ω_F lying between ω_θ and ω_ψ.

As ω_F is a weighted average of ω_θ and ω_ψ, one might expect ω_F to be a more accurate estimator of the true frequency ω_T. This hope is dampened when one realizes that the deviations of ω_θ and ω_ψ from the true frequency ω_T are strongly positively correlated.

Downloaded from https://academic.oup.com/gji/article/91/3/755/641480 by guest on 21 August 2022

The correlation between ω_θ and ω_ψ can be estimated as

$$\langle(\omega_\theta - \omega_T)(\omega_\psi - \omega_T)\rangle \approx \frac{\langle\psi'(\omega_T)\theta'(\omega_T)\rangle}{\langle\psi''(\psi_T)\theta''(\omega_T)\rangle}, \tag{A.38}$$

where

$$\langle\psi'(\omega_T)\theta'(\omega_T)\rangle = \rho\,\{\sigma_N^4 \operatorname{tr}(\tilde{\mathbf{M}}^{(2)} \cdot \mathbf{\Gamma}^{(1)}) + \sigma_N^2 |\mu|^2 \sum_{t=0}^{N-1} (\mathbf{M}^{(1)} \cdot \hat{\mathbf{v}})_t (\mathbf{M}^{(1)} \cdot \mathbf{\Gamma}^{[0,\alpha]})_{tt} \hat{v}(t) \exp(-\alpha t)\} \tag{A.39}$$

and

$$\langle\psi''(\omega_T)\theta''(\omega_T)\rangle = \rho\,\{\sigma_N^4 \operatorname{tr}(\tilde{\mathbf{M}}^{(4)} \cdot \mathbf{\Gamma}^{(1)}) + 2\sigma_N^2 |\mu|^2 \sum_{t=0}^{N-1} (\mathbf{M}^{(2)} \cdot \hat{\mathbf{v}})_t (\mathbf{M}^{(2)} \cdot \mathbf{\Gamma}^{[0,\alpha]})_{tt} \hat{v}(t) \exp(-\alpha t) + |\mu|^4 (\hat{\mathbf{v}} \cdot \mathbf{M}^{(2)} \cdot \hat{\mathbf{v}}) \operatorname{tr}(M^{(2)} \cdot \mathbf{\Gamma}^{[\alpha,\alpha]})\}, \tag{A.40}$$

where $\tilde{\mathbf{M}}^{(j)}$ has elements

$$\tilde{M}_{kl}^{(j)} = M_{kl}^{(j)} \hat{v}(k) \exp(\alpha k) \hat{v}(l) \exp(\alpha l), \qquad k, l = 0, 1, 2, \ldots, N-1$$

Using these equations one finds that the cross-correlation of ω_θ and ω_ψ is almost unity. For example, if $\beta = \nu = 0$ and $N|\mu|^2/\sigma_N^2 = 10$, $\langle(\omega_\theta - \omega_T)(\omega_\psi - \omega_T)\rangle = 0.922$. Any averaging of the two estimators ω_θ and ω_ψ will not result in an estimator which has significantly less error associated with it.

Using (A.34), one can see that for large values of F, $\omega_F \approx \omega_\psi$. Therefore, we estimate the errors in the frequencies of the F-test peaks using equation (A.27).

A3 Detection sensitivity

It is useful to know the sensitivity of the F-test to the presence of a decaying sinusoid of frequency ω_T. The signal-to-noise ratio required for detection of a sinusoid at a given confidence level can be calculated. Suppose that the time series is given by (A.1), with μ either purely real or purely imaginary. It can be shown that at frequency ω_T the random variable F defined in (3.28) follows a noncentral F-distribution with noncentrality parameter

$$\gamma = \frac{2|\mu|^2}{\sigma_N^2} \sum_{k=0}^{K-1} |V_k(0; \beta, \nu)|^2 \tag{A.41}$$

(Kendall & Stuart 1979). The expected value of $F(\omega_T)$ is

$$\langle F(\omega_T)\rangle = \frac{(2+\gamma)(K-1)}{2(K-2)} \tag{A.42}$$

(Kendall & Stuart 1979, p. 279).

In Fig. A2, $\langle F(\omega_T)\rangle$ is plotted as a function of signal-to-noise ratio for sets of five tapers with parameters $\Omega N = 8\pi$, $\beta = 0.6$, 1.05 and $\nu = 0$, 0.01, 0.1, and 1. For a given signal-to-noise ratio, the expected value of the F-test grows with increasing ν, reaching a maximum

Downloaded from https://academic.oup.com/gji/article/91/3/755/641480 by guest on 21 August 2022

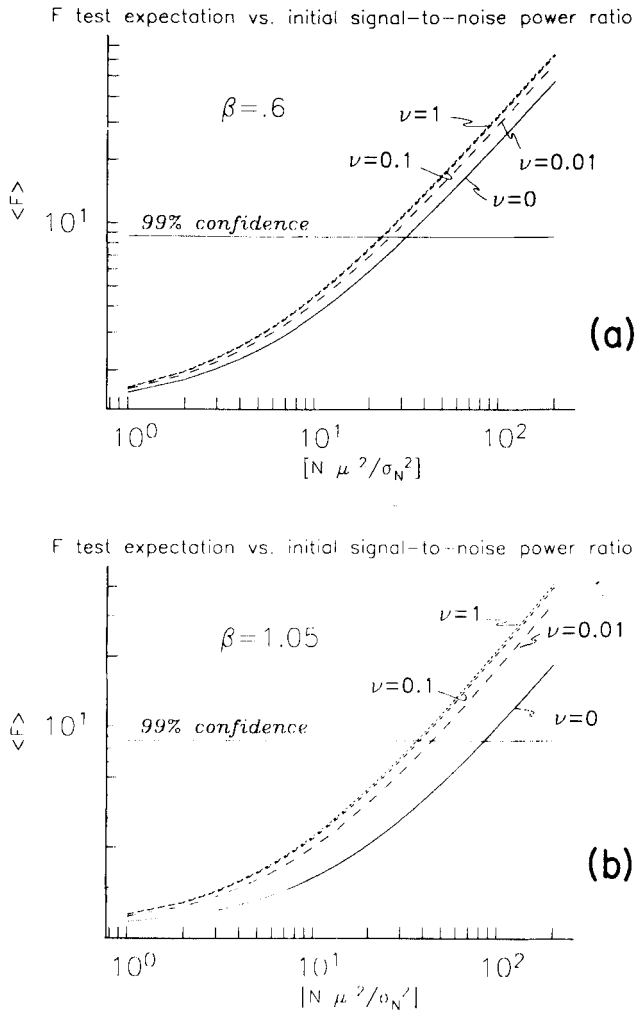

Figure A2 (a, b). Expected value of the F-test at the true frequency ω_T as a function of $N|\mu|^2/\sigma_N^2$ for five tapers with $\Omega N = 8\pi$, $\beta = 0.6$ and $\beta = 1.05$, and $\nu = 0$, 0.01, 0.1 and 1. Larger values of ν are plotted with increasingly shorter dashes. The 99 per cent confidence level for an F-distributed random variable with 2 and 8 degrees of freedom ($F = 8.65$) is shown. For a given initial signal-to-noise ratio, $\langle F \rangle$ increases as ν increases. Therefore, it is easier to detect a decaying sinusoid using tapers designed with large values of the noise parameter ν.

when $\nu = 1$. Suppose one wants to detect a decaying sinusoid at the 99 per cent confidence level. To do this using tapers which have $\beta = 0.6$ and $\nu = 0$ requires a 25 per cent higher signal-to-noise ratio than performing the analysis with tapers which have parameters $\beta = 0.6$ and $\nu = 0.1$. Using tapers with $\beta = 1.05$ and $\nu = 0$, a 125 per cent larger value of $|\mu|^2/\sigma_N^2$ is required than employing tapers designed with $\beta = 1.05$ and $\nu = 0.1$. There is a tradeoff between detection capability (Fig. A2) and frequency uncertainty (Fig. A1), but tapers designed with $0.01 \lesssim \nu \lesssim 1$ provide reasonable performance in both areas.

For comparison, consider the spectral estimate obtained by taking the discrete Fourier transform of a time series which has been multiplied by a cosine taper. A cosine taper

Downloaded from https://academic.oup.com/gji/article/91/3/755/641480 by guest on 21 August 2022

$w_c(t)$ is defined by

$$w_c(t) = A\left[1 - \cos\left(\frac{2\pi t}{N-1}\right)\right]; \qquad t = 0, 1, \ldots, N-1, \tag{A.43}$$

where A is chosen so that

$$\sum_{t=0}^{N-1} [w_c(t)]^2 = 1.$$

A direct estimate of the spectrum of the data $x(t)$ is $|y_c(w)|^2$, where

$$y_c(\omega) = \sum_{t=0}^{N-1} \exp(-i\omega t)\, w_c(t)\, x(t). \tag{A.44}$$

The peak frequency ω_c defined by

$$\frac{d}{d\omega}|y_c(\omega)|^2\Big|_{\omega=\omega_c} = 0 \tag{A.45}$$

is taken as the estimator of the true frequency ω_T of a sinusoidal signal in the data. As before, ω_c is an unbiased estimator of ω_T, and it has mean-square error

$$\langle(\omega_c - \omega_T)^2\rangle \approx \frac{\left\langle\left(\frac{d}{d\omega}|y_c(\omega)|^2\right)^2\Big|_{\omega=\omega_T}\right\rangle}{\left\langle\left(\frac{d^2}{d\omega^2}|y_c(\omega)|^2\right)^2\Big|_{\omega=\omega_T}\right\rangle} \tag{A.46}$$

Expressions for the expectations on the right-hand side of (A.46) are identical to (A.17) and (A.18) with $w_c(t)\exp(-\alpha t)$ replacing $\hat{v}(t)$, and $\rho = 1$.

For data consisting only of Gaussian white noise, $2|y_c(\omega)|^2/\sigma_N^2$ is χ^2 distributed with two degrees of freedom, and there is a probability of 0.01 that $2|y_c(\omega)|^2/\sigma_N^2$ will reach or exceed 9.21 (Abramowitz & Stegun 1965). If $|y_c(\omega)|^2$ exceeds the value $9.21\,\sigma_N^2/2$ at some frequency, then one is more than 99 per cent confident that a signal exists at that frequency. It is easy to show that, for the time series (A.1),

$$\langle|y_c(\omega_T)|^2\rangle = |\mu|^2\left(\sum_{t=0}^{N-1} w_c(t)\exp(-\alpha t)\right)^2 + \sigma_N^2 \tag{A.47}$$

so that

$$N|\mu|^2/\sigma_N^2 \cong 3.6N\left(\sum_{t=0}^{N-1} w_c(t)\exp(-\alpha t)\right)^{-2} \tag{A.48}$$

is the value of the initial signal-to-noise power ratio associated with 99 per cent detection confidence at frequency ω_T.

Suppose one wants to detect a decaying sinusoid with decay parameter $\beta = 0.6$ (or decay rate $\alpha = 0.6\pi/T$) at the 99 per cent confidence level. Using the spectral estimate $|y_c(\omega)|^2$, a value of $N|\mu|^2/\sigma_N^2$ of approximately 32 is required, whereas using an F-test and five tapers for $\beta = 0.6$, $\nu = 0.1$, $N|\mu|^2/\sigma_N^2 \approx 23.5$ corresponds to detection at the 99 per cent confidence level. If the decaying sinusoid has a decay parameter of $\beta = 1.05$, an initial signal-

Downloaded from https://academic.oup.com/gji/article/91/3/755/641480 by guest on 21 August 2022

to-noise ratio of $N|\mu|^2/\sigma_N^2 \approx 104$ is needed for 99 per cent confidence level detection using the spectral estimate $|y_c(\omega)|^2$, but $N|\mu|^2/\sigma_N^2$ only needs to be 38 when the multitaper method is applied, using five tapers with $\beta = 1.05$ and $\nu = 0.1$. In this case, the multitaper approach is 274 per cent more efficient then the cosine-taper spectral method.

Clearly, the spectral estimate $|y_c(\omega)|^2$ is a less sensitive detector of decaying sinusoids in a time series than the multitaper method. Much of this discrepancy in detection ability is due to the eigentaper's preferential weighting of the start of the record where the signal-to-noise ratio is greater. Also, more information is extracted from a given time-series by applying several tapers; the extra degrees of freedom allow a better-constrained least-squares fit of the decaying sinusoid model to the data. Another advantage of the multiple-taper technique is that it allows one to discriminate between signals which are truly harmonic, and those which have time varying phases; conventional spectral estimates employing single tapers do not.

The variance of the random variable $F(\omega_T)$ can also be expressed in terms of the non-centrality parameter γ defined in (A.41);

$$\text{var}\,[F(\omega_T)] = \frac{(K-1)^2\,[4(\gamma+1)(K-1)+\gamma^2]}{8(K-2)^2(K-3)} \tag{A.49}$$

when the data are given by (A.1), and μ is purely real or purely imaginary. The height of an F-test peak is not very well determined; $\sqrt{\text{var}\,[F(\omega_T)]} \geqslant {}^1/_3\langle F(\omega_T)\rangle$ when $K = 5$ for values of F above the 90 per cent detection threshold.

Downloaded from https://academic.oup.com/gji/article/91/3/755/641480 by guest on 21 August 2022